RadioGraphics

From the Radiologic Pathology Archives[1]

Ewing Sarcoma Family of Tumors: Radiologic-Pathologic Correlation[2]

Mark D. Murphey, MD • Lien T. Senchak, MD • Pramod K. Mambalam, MD • Chika I. Logie, MD • Mary K. Klassen-Fischer, MD • Mark J. Kransdorf, MD

SA-CME

See www.rsna.org/education/search/RG

LEARNING OBJECTIVES FOR TEST 4

After completing this journal-based SA-CME activity, participants will be able to:

- Describe the spectrum of radiologic findings in the Ewing sarcoma family of tumors.
- Discuss the pathologic basis for the radiologic features of the Ewing sarcoma family of tumors.
- Recognize the radiologic appearance after neoadjuvant chemotherapy and the pattern of metastatic disease in the Ewing sarcoma family of tumors.

TEACHING POINTS

See last page

The Ewing sarcoma family of tumors includes osseous Ewing sarcoma, extraskeletal Ewing sarcoma, primitive neuroectodermal tumor, and Askin tumor. They share a karyotype abnormality with translocation involving chromosomes 11 and 22. Histologically, these lesions demonstrate crowded sheets of small round blue cells. Imaging features of osseous Ewing sarcoma often suggest the diagnosis, with aggressive long-bone destruction in the metadiaphysis of an adolescent or young adult and an associated soft-tissue mass. Focal areas of cortical destruction are frequent, allowing continuity between the intraosseous and extraosseous components. This continuity is also commonly seen as subtle channels extending through the cortex at computed tomography or magnetic resonance (MR) imaging, a finding that reflects the underlying pathologic appearance. Extraskeletal Ewing sarcoma commonly demonstrates a nonspecific radiologic appearance of a large soft-tissue mass affecting the paraspinal region or lower extremity. Askin tumor represents extraskeletal Ewing sarcoma involving the chest wall. Imaging typically reveals a large pleural-based mass and associated pleural effusion. Treatment of these tumors is usually a combination of neoadjuvant chemotherapy followed by surgical resection, which may be supplemented with radiation therapy. Imaging, particularly MR, is also vital to evaluate response to neoadjuvant therapy, direct surgical resection, and detect local recurrence or metastatic disease.

Abbreviations: FDG = fluorine 18 fluorodeoxyglucose, H-E = hematoxylin-eosin, PNET = primitive neuroectodermal tumor, RT = radiation therapy, SUV = standardized uptake value, TR = repetition time

RadioGraphics 2013; 33:803–831 • **Published online** 10.1148/rg.333135005 • **Content Codes:** MK MR OI PD

[1]Supported by the American Institute for Radiologic Pathology (AIRP), the Joint Pathology Center (JPC), and Uniformed Services University of the Health Sciences (USU).

[2]From the Musculoskeletal Section, American Institute for Radiologic Pathology, 1010 Wayne Ave, Suite 320, Silver Spring, MD 20910 (M.D.M., L.T.S., P.K.M., C.I.L.); Uniformed Services University of the Health Sciences, Bethesda, Md (M.D.M., C.I.L.); Department of Radiology, Walter Reed National Military Medical Center, Bethesda, Md (M.D.M.); the Joint Pathology Center, Silver Spring, Md (M.K.K.F.); and Department of Radiology, Mayo Clinic Hospital, Phoenix, Ariz (M.J.K.). Received January 23, 2013; revision requested February 12; revision received March 11; accepted March 13. For this journal-based SA-CME activity, the authors, editor, and reviewers have no relevant relationships to disclose. **Address correspondence to** M.D.M. (e-mail: *mmurphey@acr.org*).

The opinions and assertions contained herein are the private views of the authors and are not to be construed as official or as representing the views of the Departments of the Army, Navy, Air Force, or Defense.

Introduction

James Ewing described the tumor that would eventually bear his name as diffuse endothelioma of bone in 1921 and later as endothelial myeloma (1). He described the lesion as "differing markedly from osteogenic sarcoma [or] any known form of myeloma and ... designated by the vague term round cell sarcoma of unknown origin and nature" and suggested the probable endothelial origin of this neoplasm. Dr Ewing was appointed as the first professor of pathology at Cornell University in 1899 and had extensive interest in and experience with osseous tumors. He cofounded the American Society for the Control of Cancer (now the American Cancer Society) in 1913. His extensive research on cancer and its treatment led to him being on the cover of *Time* magazine in 1931 as "Cancer Man Ewing."

The initial theory of the cell origin of Ewing sarcoma included the endothelial cells and undifferentiated mesenchymal cells of bone marrow. The advent of immunohistochemistry and cytogenetic evaluation suggested a neuroectodermal origin. Although Ewing sarcoma was initially described in bone, an extraskeletal location was reported in 1975 by Angervall and Enzinger (2). Subsequently, lesions in bone and soft tissue with microscopic features indistinguishable from those of Ewing sarcoma, but with histologic rosette formation and other pathologic features of neural differentiation, were described as primitive neuroectodermal tumor (PNET) (3,4). Askin and colleagues (5) reported a similar series of lesions involving the chest wall, referred to as Askin tumors, in 1979. Thus, there appeared to be two distinct but similar lesions, Ewing sarcoma and PNET (including Askin tumor), that involved bone or soft tissue.

The advent of cytogenetic evaluation of lesions demonstrated that Ewing sarcoma, PNET, and Askin tumor all shared a common karyotype abnormality. This translocation between the long arms of chromosomes 11 and 22 (t[11;22][q24;q12]) is present in approximately 90% of these lesions (6,7). Subsequent development of additional and more sophisticated cytogenetic and molecular evaluation techniques has confirmed the common genetic lineage of these tumors. Furthermore, Cavazzana and coworkers (8) were able to induce neural differentiation in Ewing sarcoma in vitro. Thus, it is now nearly universally agreed that Ewing sarcoma, PNET, and Askin tumor are cytogenetically closely related if not identical lesions on a morphologic continuum, which is referred to as the Ewing sarcoma family of tumors.

Teaching Point

In this article, we review the clinical features, pathologic appearance, and imaging characteristics of the Ewing sarcoma family of tumors. Treatment and prognosis of these tumors and posttreatment imaging are also discussed.

Ewing Sarcoma of Bone

Clinical Characteristics

Ewing sarcoma of bone represents the second most common primary malignant tumor of bone in children and adolescents, exceeded in prevalence only by osteosarcoma (6,9–11). Overall, it is the fourth most frequent primary malignant tumor of bone after multiple myeloma, osteosarcoma, and chondrosarcoma (6,9–11). Ewing sarcoma accounts for approximately 3% of all pediatric cancers (9). The annual incidence of Ewing sarcoma in the United States is 200 cases, with a rate of one to three cases per 1 million children (12–14). Ewing sarcoma is most frequent in the first 3 decades of life, with 95% of cases reported between the ages of 4 and 25 years (14,15). The peak prevalence is between the ages of 10 and 15 years. There is a slight male predilection (male-to-female ratio, 1.5:1). There is a marked predominance of Ewing sarcoma in white patients (95% of cases); this lesion only rarely affects blacks (0.5%–2% of cases) (6,9,16).

There is a wide skeletal distribution for Ewing sarcoma. However, the most common affected sites are the femur (21% of cases), ilium (12%–13%), tibia (8%–11%), humerus (10%), fibula (7%–9%), ribs (8%), and sacrum (6%) (6,9,16). The pelvis, extremities, and ribs account for approximately 86% of cases (14,15). Other less frequently involved skeletal locations include the mobile portion of the spine (4%–6%), scapula (4%–5%), hand or foot (3%–6%), radius or ulna (3%–5%), mandible or maxilla (1%–2%), clavicle (2%), calvaria (1%), facial bones (0.5%), and sternum (0.2%) (9,15).

Long tubular bone involvement is more common proximally than distally. While a diaphyseal location of osseous Ewing sarcoma is often emphasized, the majority of long-bone lesions are actually metadiaphyseal (44%–59%) (6,9,16). Diaphyseal lesions account for 33%–35% of cases, while a Ewing sarcoma confined to the metaphysis represents 5%–15% of lesions (14). Epiphyseal extension may be seen in up to 10% of cases, although lesions centered in the epiphysis are rare (0.5%–2%) (6,9,16).

The clinical presentation of Ewing sarcoma is usually nonspecific, with pain (82%–88% of patients) and a mass or swelling (60% of patients) (17–20). Symptoms are often present for more than 6 months before diagnosis. Fever (20%–49% of patients) and increased erythrocyte sedimentation rate (43% of patients) simulat-

Figure 1. Gross pathologic and histologic appearance of Ewing sarcoma of bone. **(a)** Drawing of the proximal femur shows intramedullary involvement by tumor *(M)* extending into the soft tissue *(T)* through focal cortical destruction (arrows). **(b)** Drawing reveals intramedullary tumor *(M)* permeating through the haversian canals and neurovascular channels (arrowheads). This pattern of extension allows continuity between the medullary *(M)* and soft-tissue *(T)* components without large areas of focal cortical destruction. **(c)** Photomicrograph (original magnification, ×250; hematoxylin-eosin [H-E] stain) demonstrates monotonous round blue cells typical of Ewing sarcoma. There is mild pseudorosette formation (circles). Inset (upper left corner) (original magnification, ×450) reveals typical indistinct cell membranes, indented nuclei, and scant cytoplasm. (Fig 1a and 1b courtesy of Aletta Ann Frazier, MD, American Institute for Radiologic Pathology, Silver Spring, Md, and University of Maryland School of Medicine, Baltimore, Md.)

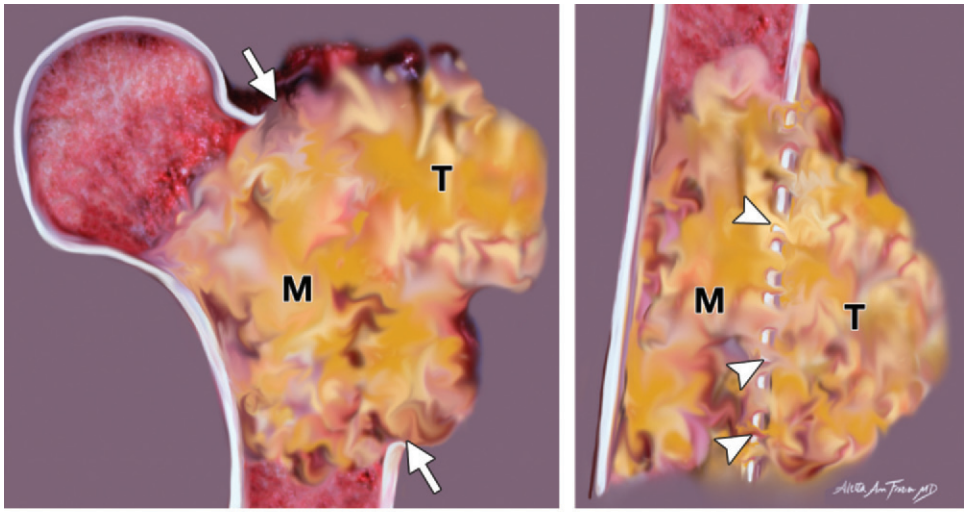

a. b.

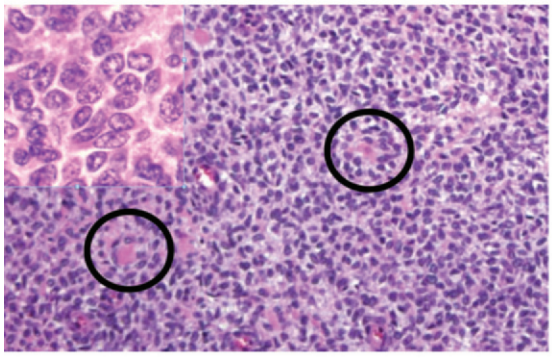

c.

ing an infectious origin are also common clinical features in Ewing sarcoma patients at presentation, often correlating with advanced disease and metastases (14,17,20). Pathologic fractures are uncommon as an initial clinical presentation (17,20). Additional clinical manifestations are related to the site of involvement and include neurologic symptoms (spine and calvarial lesions), pleuritic chest pain (rib lesions), dental abnormalities (facial lesions), and gait disturbances (lower long-bone lesions).

Pathologic Features

At gross pathologic evaluation, Ewing sarcoma is a soft gray-to-white mass that often has relatively well-defined margins, although poorly defined margins may also be present. Osseous lesions originate in the central medullary canal, with early involvement of the soft tissues in 80%–100% of cases (6,9,10). Soft-tissue masses are usually large and circumferential about the involved bone; they may exceed the intraosseous component in size in 2%–15% of cases (9,16). The communication between the medullary canal and soft-tissue components may be through focal cortical destruction (Fig 1). However, in our experience, it is more commonly through permeation of the cortical haversian canal system and along neurovascular channels with small nests of tumor cells (Fig 1). Periosteal elevation is common.

Histologic sections show crowded sheets of small round blue cells or lobules of such cells divided by a small amount of fibrous stroma. The cells range from 10 μm to 15 μm in diameter and have scant clear cytoplasm and indistinct cell membranes. The nuclei are round with indentations of the nuclear membrane and small nucleoli. The cells may also form Homer-Wright rosettes, in which they are arranged around a central fibrous core, or pseudorosettes, with arrangement around a central blood vessel. Historically, greater than 20% of tumor tissue showing this rosette formation was used as a criterion for diagnosis of PNET, although this extent is rare (6,21).

There may be areas of hemorrhage or necrosis with ghost cells. However, extensive necrosis is uncommon before treatment. The number of mitotic figures is quite variable but typically not numerous. New bone formation, often seen on devitalized bone, has also been described within the medullary canal (22). Histologic variants of this classic Ewing sarcoma include large cell subtype and those with adamantinoma-like features (6,9,23,24). After treatment, tumor cells may show pleomorphic changes including formation of tumor giant cells, extensive necrosis, and osteoid mineralization.

The cytoplasm of the Ewing sarcoma tumor cells usually contains glycogen; therefore, they are periodic acid–Schiff stain positive (70%–100%) and diastase-sensitive (6,9,25). Immunohistochemical staining for CD99 (MIC2), neuron-specific enolase, Leu7 (CD57), FL-1 protein, and vimentin is usually positive (26,27). The MIC2 gene product is present in 90% of Ewing sarcomas (6,9,21). Tumor cells may also be positive for low-molecular-weight keratins or synaptophysin. Tumor cells are negative for S100, leukocyte common antigen (CD45), muscle markers, and vascular markers.

The pathologic differential diagnosis includes other small round blue cell tumors, such as metastatic neuroblastoma, non-Hodgkin lymphoma, desmoplastic small round cell tumor, embryonal rhabdomyosarcoma, small cell osteogenic sarcoma, other primitive neuroectodermal tumors, and poorly differentiated synovial sarcoma, which can usually be distinguished by the immunohistochemical staining pattern and cytogenetic or molecular genetic testing (28). Electron microscopy is not routinely performed; however, it demonstrates limited cytoplasmic organelles, glycogen, lack of true desmosomes, and rare dense core granules.

Cytogenetic evaluation is an essential component of the diagnostic and prognostic evaluation of Ewing sarcoma (11,29). The typical cytogenetic aberration, identified in 85%–95% of lesions, is the nonrandom reciprocal translocation between chromosomes 11 and 22 (t[11;22][q24;q12]) (6,9–11,29,30). The 22q12 locus codes for *EWS*, a transcription factor, while the 11q24 site codes for *FLI1* (6,9–11,30). The *EWS-FLI1* fusion transcript, seen in approximately 85% of cases, acts as a transactivator of the c-Myc promoter (9,29–31). Another cytogenetic aberration, seen in only 5%–10% of Ewing sarcomas, is the translocation t(21;22)(q22;q12), which is referred to as *EWS-ERG* (6,9,29,30). The fusion protein derived from *EWS-ERG* is similar to that of the *EWS-FLI1* gene product.

Teaching Point

Other translocations more rarely encountered in Ewing sarcoma include t(7;22)(p22;q12) *EWS-ETV1*, t(17;22)(q12;q12) *EWS-E1AF*, and t(2;22)(q33;q12) *EWS-FEV* (6,9). These translocations may be detected by conventional G banding; however, molecular genetic techniques, such as reverse transcriptase polymerase chain reaction and fluorescent in situ hybridization, may be more sensitive and accurate. These cytogenetic abnormalities and their resultant protein products may downregulate tumor suppressor genes and allow the Ewing sarcoma family of tumor cells to avoid programmed cell death (21,32).

Imaging Characteristics

At radiography, Ewing sarcoma of bone reveals aggressive features, reflecting the high-grade nature of this malignant lesion (9,18,33,34). Bone destruction with a moth-eaten to permeative pattern is seen in 76%–82% of lesions (Fig 2), and a wide zone of transition (poor margination) is seen in 96% of lesions (6,9,10,15,35). Geograph-

Teaching Point

Figure 2. Ewing sarcoma of bone in the fibular diaphysis in a 16-year-old boy with swelling, pain, and an enlarging mass in the left distal lower extremity. **(a)** Frontal radiograph shows a permeative lytic bone lesion in the distal fibular diaphysis (white oval) with aggressive hair-on-end periosteal reaction (arrows) and Codman triangles (arrowheads). **(b, c)** Axial **(b)** and sagittal **(c)** computed tomographic (CT) images of the fibula better depict both the hair-on-end aggressive periosteal reaction (arrow) and Codman triangles (white arrowheads in **c**) as well as the extensive involvement of the marrow. A pathologic fracture is also seen. No large focal areas of cortical destruction are identified, but linear channels of low attenuation are seen extending through the cortex (arrowhead in **b**, black arrowheads in **c**), which allow continuity between the medullary and soft-tissue components. **(d–f)** Axial T1-weighted (repetition time [TR] [msec]/echo time [msec] = 400/15) **(d)**, contrast-enhanced T1-weighted (617/15) **(e)**, and T2-weighted (4766/34) **(f)** magnetic resonance (MR) images demonstrate the lesion centered in the marrow canal *(M)* with circumferential soft-tissue extension *(S)*. The lesion is heterogeneously intermediate in signal intensity on both the T1-weighted and T2-weighted images with diffuse enhancement on the postcontrast image. Periosteal reaction is better seen at radiography and CT. Cortical involvement is seen as intermediate-signal-intensity channels extending through the low-signal-intensity cortex (arrowheads), allowing continuity between the medullary canal and soft-tissue components. **(g)** Photograph of the sagittally sectioned gross specimen reveals identical features as depicted at imaging with a medullary *(M)* centered lesion, aggressive periosteal reaction (curved arrows = Codman triangles, straight arrows = hair-on-end reaction), and soft-tissue extension *(S)*. Linear channels of extension through the cortex are also seen (arrowheads), allowing continuity between the medullary and soft-tissue components. Scale is in centimeters. ▶

RadioGraphics

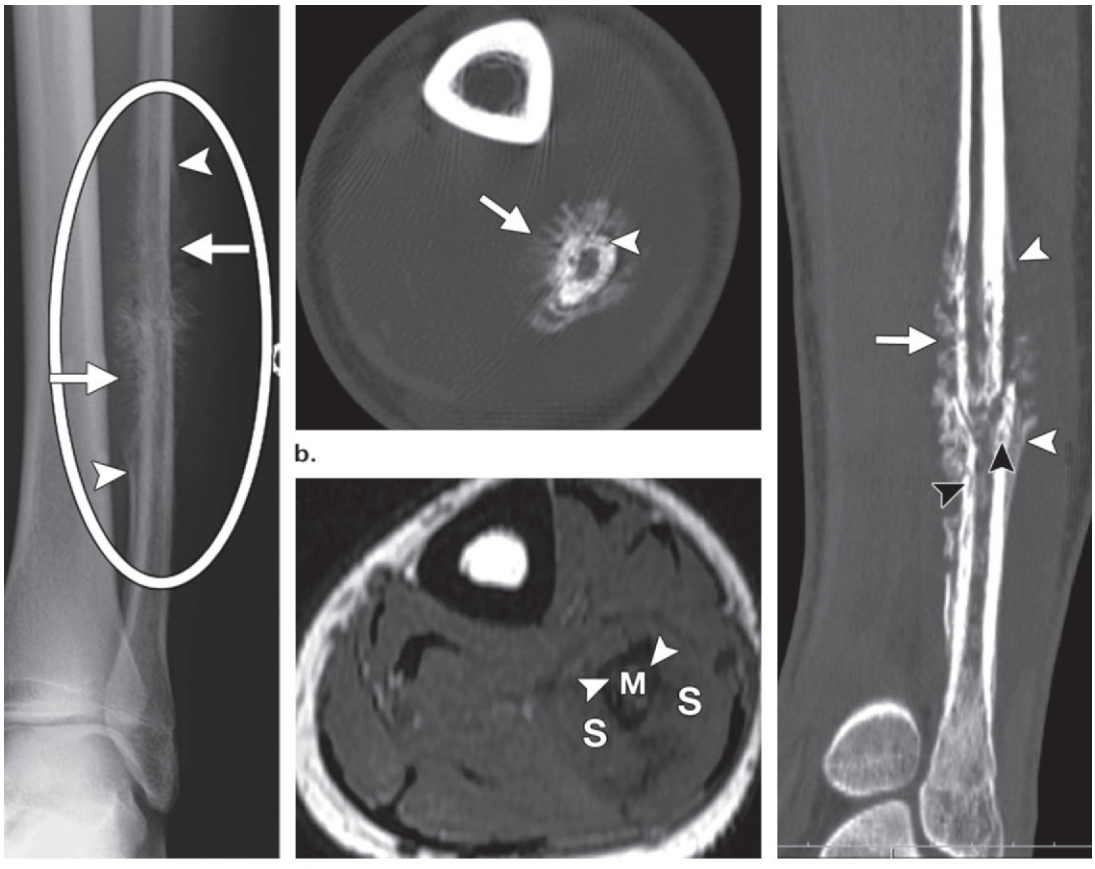

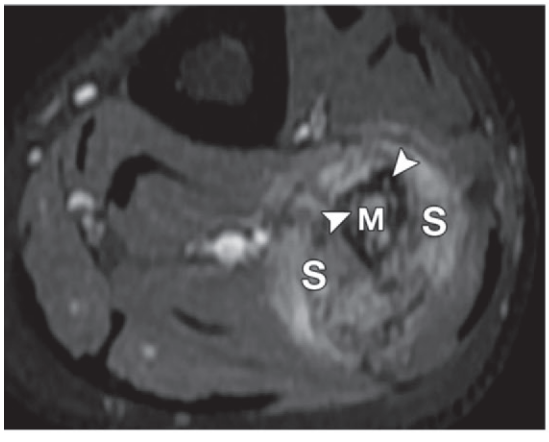

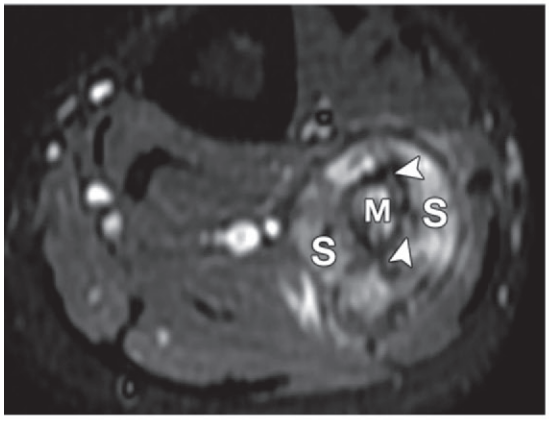

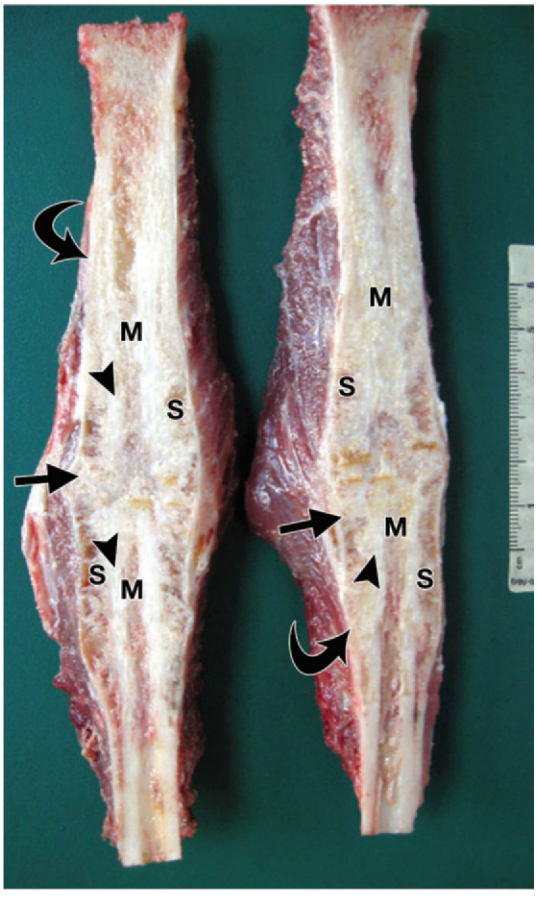

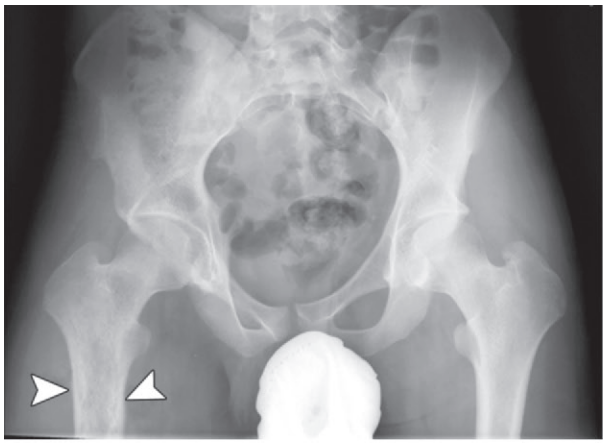

a.

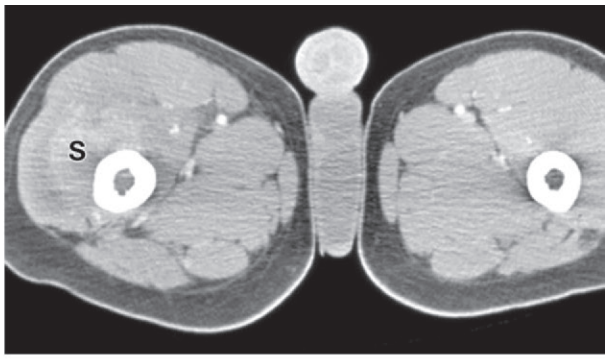

b.

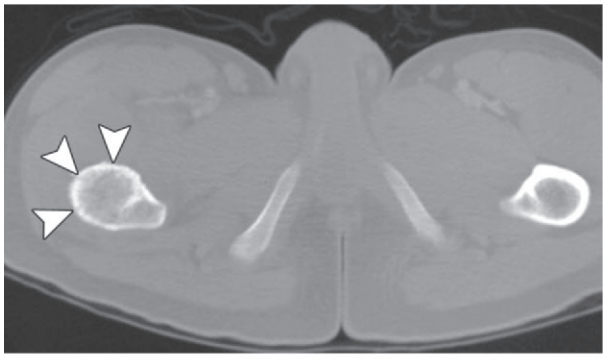

c.

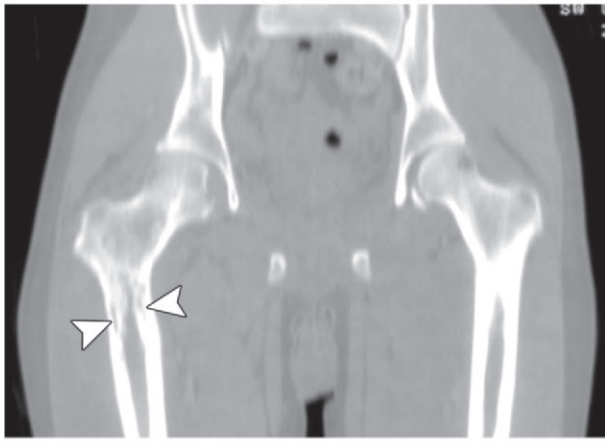

d.

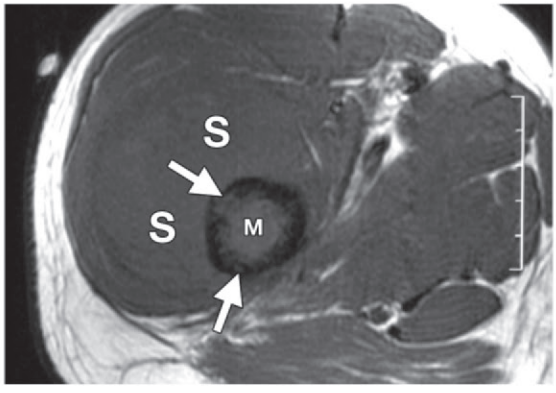

e.

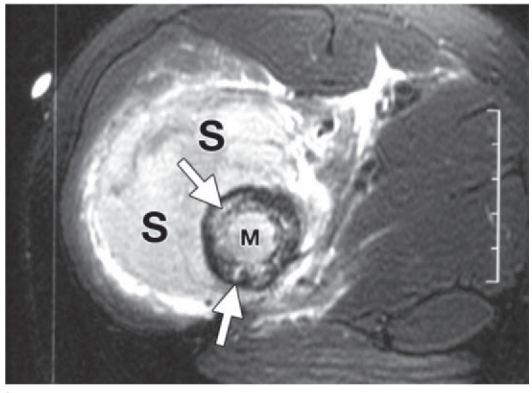

f.

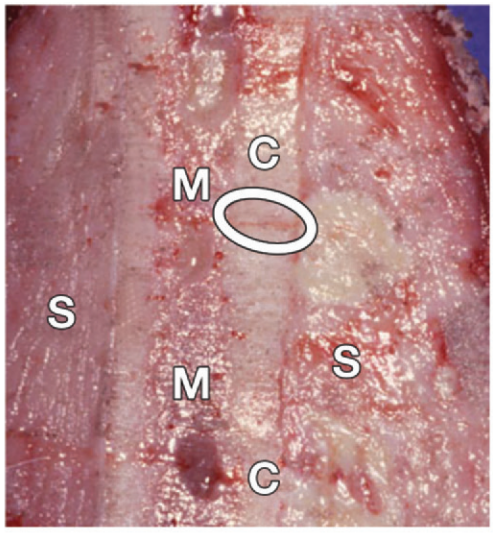

g.

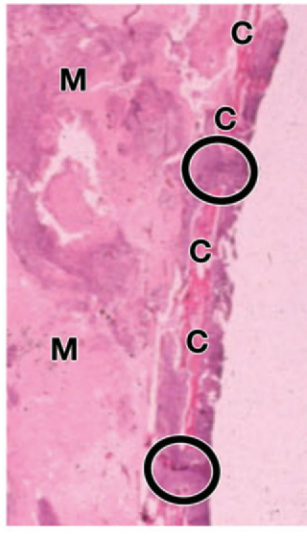

h.

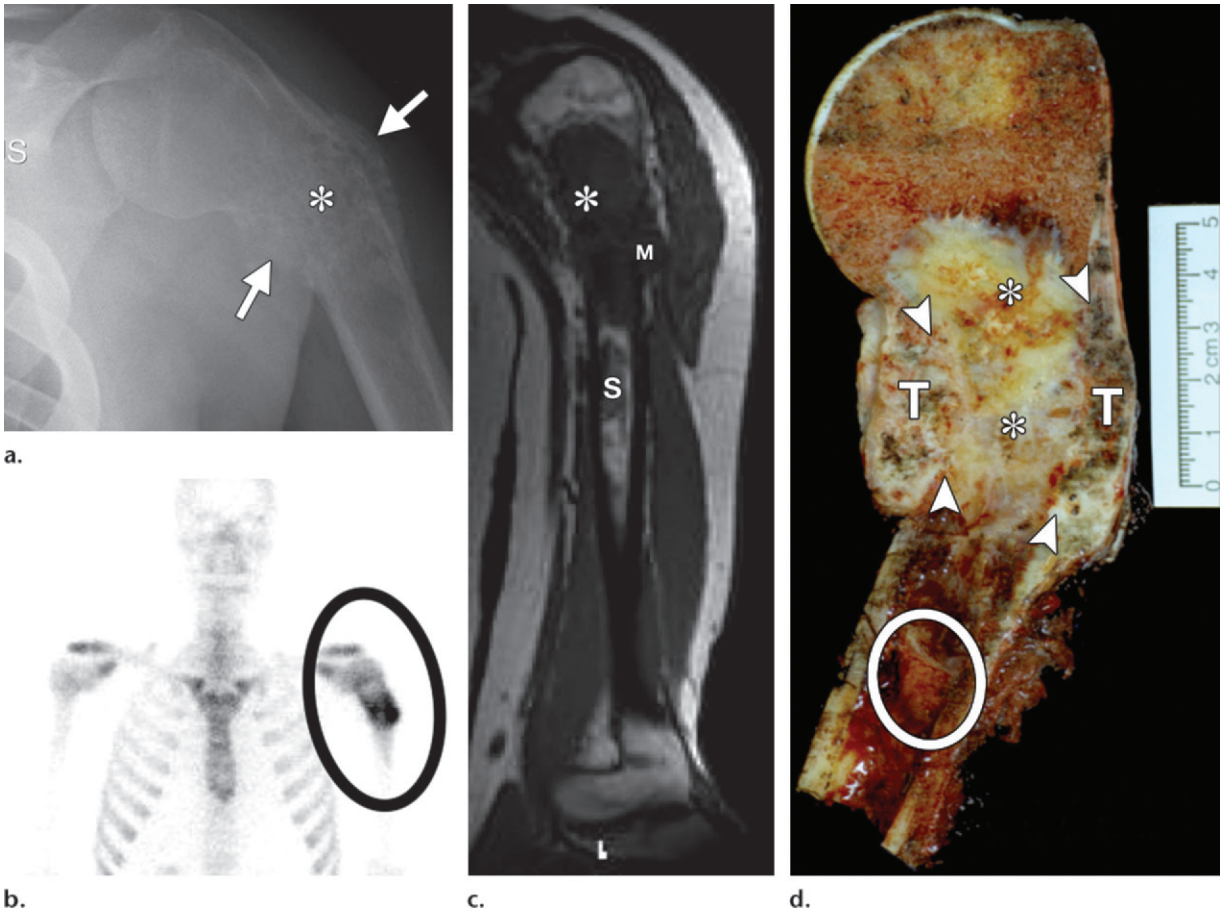

Figure 4. Ewing sarcoma of the proximal humeral metadiaphysis in a 25-year-old man with a skip metastasis. **(a)** Frontal radiograph shows a permeative lytic lesion in the proximal humeral metadiaphysis (∗) with a pathologic fracture and aggressive periosteal reaction (arrows). **(b)** Static frontal image from whole-body bone scintigraphy reveals heterogeneous markedly increased uptake of radionuclide (black oval) in the humeral lesion. **(c)** Coronal T1-weighted MR image (500/15) demonstrates focal marrow replacement in the proximal humeral lesion (∗) with focal cortical destruction and an associated soft-tissue mass *(M)*. A skip metastasis is seen as a separate focus of marrow replacement *(S)*, which is separated from the primary focus by a small area of normal intervening marrow. **(d)** Photograph of the coronally sectioned gross specimen shows the focal marrow replacement (∗), cortical destruction (arrowheads), soft-tissue extension *(T)*, and distal skip metastasis (white oval), findings that correlate with the imaging appearance. The deformity of the humerus is due to the pathologic fracture.

ic bone destruction with a wide zone of transition is seen in 15% of cases (6,9,10,15,18,35). Cortical destruction (19%–42%) with an associated soft-tissue mass (56%–80%) is also common (Fig 3) (9,15,35). Periosteal reaction is frequent (58%–84%) and usually aggressive in appearance (94%), either lamellated (onionskin) (Fig 4) or spiculated (sunburst or hair-on-end) (15).

◀ **Figure 3.** Ewing sarcoma of the proximal femoral metadiaphysis in a 16-year-old boy with thigh pain. **(a)** Pelvic radiograph shows permeative bone destruction in the proximal femoral metadiaphysis and aggressive ill-defined periosteal reaction (arrowheads). **(b–d)** Axial **(b, c)** and coronal **(d)** CT images reveal the intramedullary centered lesion with marrow replacement and an asymmetric circumferential soft-tissue mass (*S* in **b**), which is larger anterolaterally. Low-attenuation channels (arrowheads in **c** and **d**) allow continuity between the medullary and soft-tissue components without large focal areas of cortical destruction. **(e, f)** Axial MR images before (600/14) **(e)** and after (700/16) **(f)** intravenous contrast material administration also demonstrate intermediate-signal-intensity channels (arrows) extending through the low-signal-intensity cortex, allowing continuity between the intramedullary *(M)* and soft-tissue *(S)* components. **(g, h)** Photographs of the coronally sectioned gross specimen **(g)** and whole-mount specimen (H-E stain) **(h)** reveal the cortex *(C)*, medullary canal involvement *(M)*, and the soft-tissue component (*S* in **g**) with continuity, which is seen as focal channels of cortical permeation (white oval in **g**, black circles in **h**).

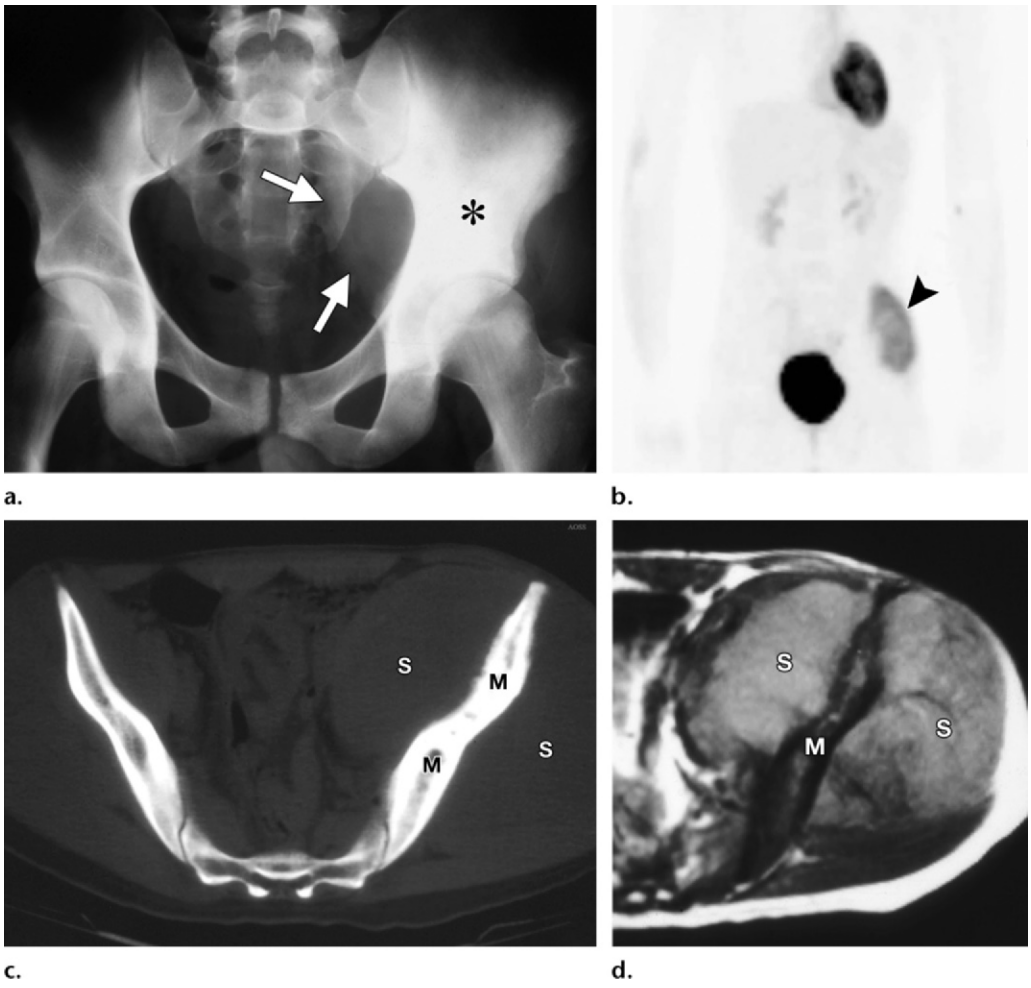

Figure 5. Ewing sarcoma of the pelvis with prominent sclerosis in a 20-year-old man. **(a)** Frontal radiograph shows a predominantly sclerotic lesion involving the left iliac bone (*) with displacement of pelvic soft tissues (arrows), suggestive of an associated soft-tissue mass. **(b)** Whole-body image from fluorine 18 fluorodeoxyglucose (FDG) positron emission tomography (PET) reveals hypermetabolic activity in the lesion (arrowhead). **(c)** Axial CT image demonstrates intramedullary sclerosis *(M)* and a large associated soft-tissue mass *(S)*, which is larger posteriorly and contains no calcification. **(d)** Axial T2-weighted MR image (2000/90) reveals the marrow involvement *(M)* with a large associated circumferential soft-tissue mass *(S)*, which is larger posteriorly and laterally and intermediate in signal intensity.

Sclerotic components are seen in 32%–40% of cases (Fig 5) (15,18,36). In our experience, these areas of sclerosis are most frequent in the intraosseous component of lesions (93%) (Fig 6) and in flat-bone lesions (18,36). Less common radiographic features of Ewing sarcoma of bone include cortical thickening (21%), pathologic fracture (15%), and expansile bone remodeling (13%) (Fig 4) (9,15,18,36). Unusual radiographic manifestations of Ewing sarcoma of bone include soft-tissue calcification (7%–9%), extrinsic cortical erosion or saucerization (6%), honeycomb appearance (6%), vertebra plana (6%), and a well-marginated lesion (4%) (9,15,37).

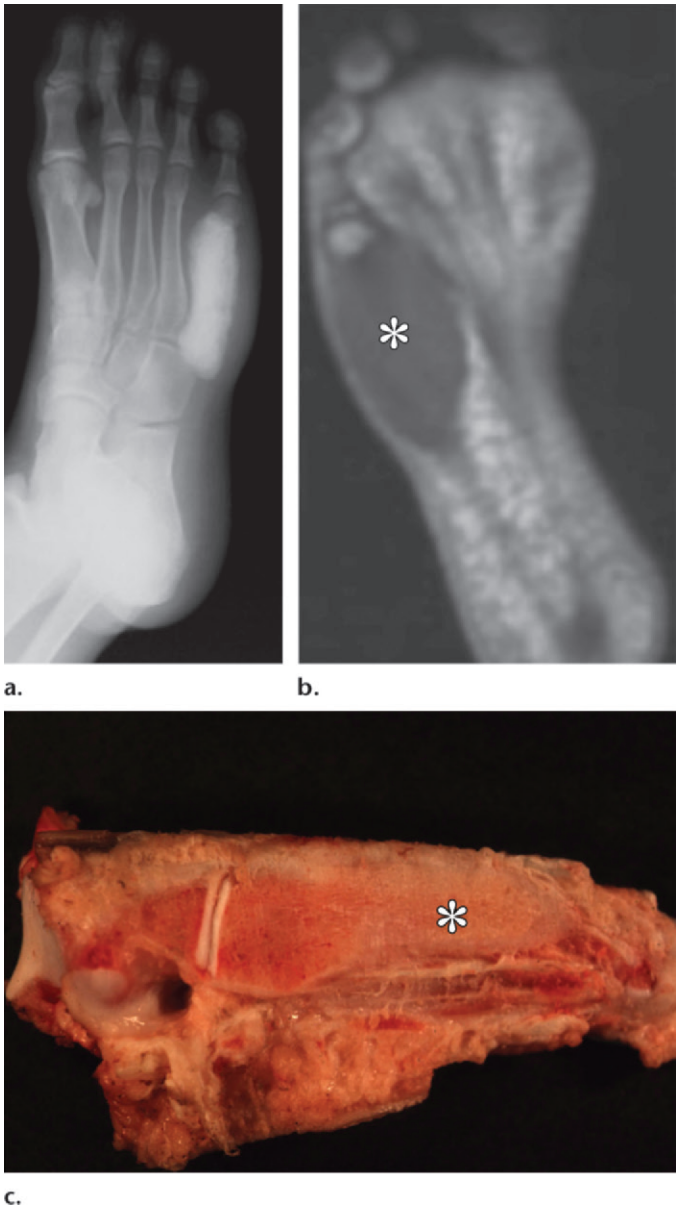

Figure 6. Ewing sarcoma in the metatarsal with prominent sclerosis in a 12-year-old boy. **(a)** Frontal radiograph shows a densely sclerotic bone lesion in the fifth metatarsal with medullary expansion. **(b)** Long-axis T1-weighted MR image (500/20) shows replacement of the fatty marrow of the fifth metatarsal with soft-tissue extension (*). **(c)** Photograph of the sagittally sectioned gross specimen of the foot shows diffuse replacement of the marrow of the fifth metatarsal with increased tissue density (*), which represents the sclerosis seen at radiography.

The moth-eaten or permeative osseous destruction typically seen in Ewing sarcoma of bone may be subtle at radiography, and a soft-tissue mass may be the predominant abnormality. Saucerization or extrinsic erosion of the bone outer cortex is more often seen in cases extending from the medullary canal. However, this medullary origin may be difficult to detect at radiography and is more optimally seen with CT and MR imaging. Periosteal Ewing sarcoma without involvement of the medullary canal is rare (3% of cases) but can also cause extrinsic erosion of bone and have a radiographic appearance similar to that of periosteal osteosarcoma (Fig 7) (38).

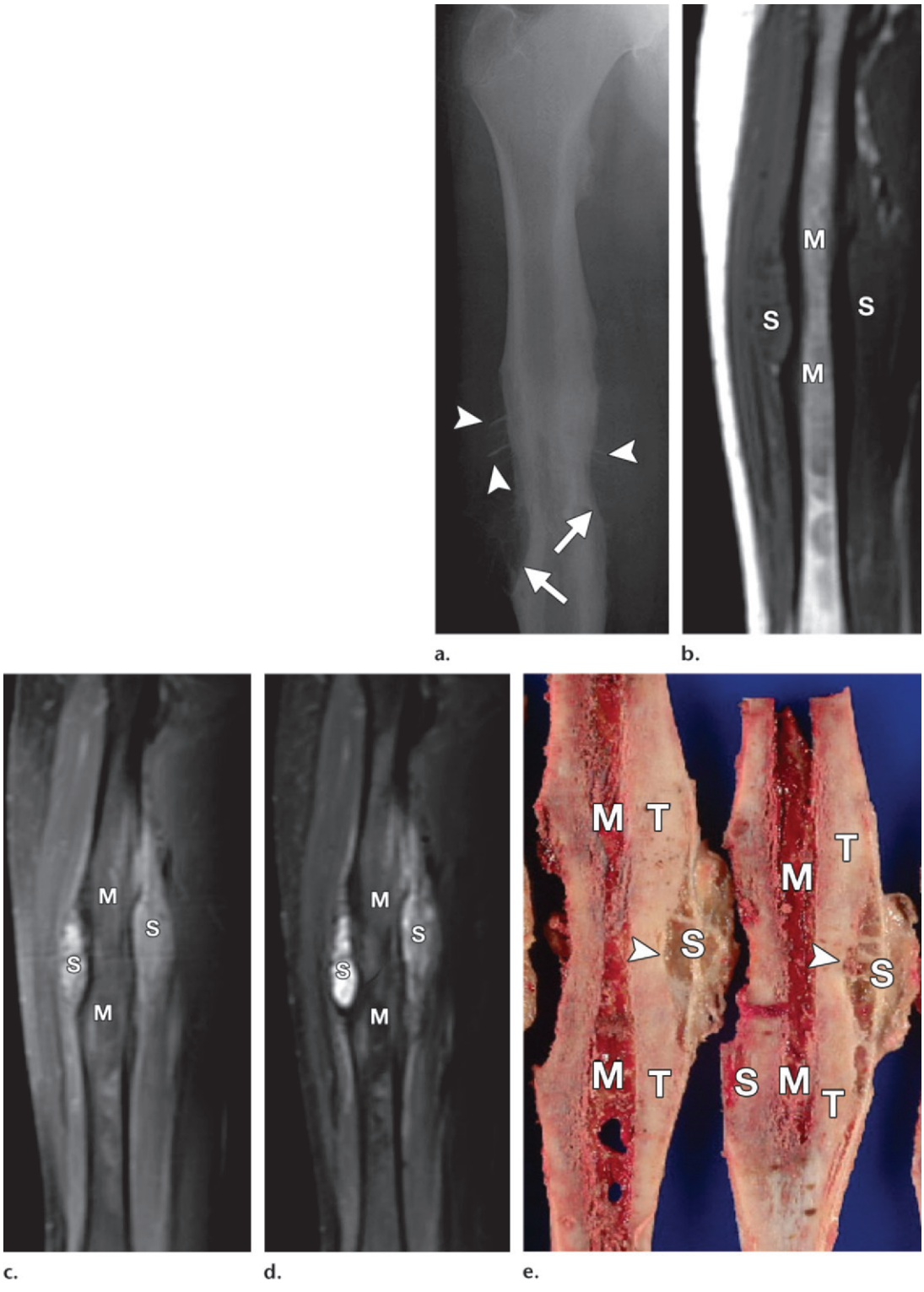

Figure 7. Periosteal Ewing sarcoma of the femoral diaphysis in a 14-year-old boy with pain in the right thigh. **(a)** Frontal radiograph shows an apparent permeative lytic bone lesion in the mid femoral diaphysis with hair-on-end periosteal reaction (arrowheads) and extrinsic erosion of the thickened cortex (arrows). **(b–d)** Sagittal T1-weighted (466/16) **(b)**, postcontrast fat-suppressed T1-weighted (700/9) **(c)**, and T2-weighted (4366/42) **(d)** MR images reveal a periosteal soft-tissue mass *(S)* without marrow involvement *(M)*. The mass demonstrates nonspecific intermediate signal intensity on the T1-weighted image, diffuse enhancement, and heterogeneous but predominantly high signal intensity on the T2-weighted image. There are mild areas of marrow abnormality with all pulse sequences, but the signal intensity is not as high as that of the soft-tissue mass on T2-weighted images. This did not represent tumor at pathologic evaluation and was presumed to be reactive or red marrow. **(e)** Photograph of the sagittally sectioned gross specimen demonstrates identical features as shown at imaging, with a subperiosteal soft-tissue mass *(S)* without marrow involvement *(M)*. Cortical thickening *(T)* and extrinsic bone erosion (arrowheads) are also seen.

The intraosseous sclerosis associated with Ewing sarcoma arising in bone typically has an osteoid appearance (dense, cloudlike), represents reactive bone formation, and is more frequent in lesions affecting flat bones, the hands or feet, and the ribs (15,18,22,36,39). Spinal lesions superior to the sacrum (ie, in the mobile portion of the spine) most commonly affect the lumbar (53%) or thoracic (22%) segments (34,40–42). These lesions are more frequently centered in the posterior elements (70%) with extension into the vertebral body (86%), while only 30% are primarily within the vertebrae (with extension into the posterior elements in 83%) (42). Spinal lesions typically reveal a large associated soft-tissue mass with spinal canal invasion (91%) (42–47).

Nuclear medicine studies show increased radionuclide uptake at both bone scintigraphy and gallium scanning (Fig 4). Blood flow, blood pool, and delayed static images reveal increased radionuclide uptake at bone scintigraphy with only rare reports of photopenia (9,48). FDG PET also shows increased radionuclide uptake in the primary lesion, with a mean maximum standardized uptake value (SUV) ranging from 5.3 (no metastases at presentation) to 11.3 (metastases at presentation) (Fig 5) (47–50). Coupled with the significantly improved spatial resolution of CT, FDG PET has been shown to demonstrate high accuracy, sensitivity, and specificity in staging and restaging of the Ewing sarcoma family of tumors (51). FDG PET is superior to bone scintigraphy in identification of osseous metastases in Ewing sarcoma (37%–88% sensitivity) and in primary bone sarcomas in general (18% not evident at bone scintigraphy in comparison with FDG PET) (48,52).

The appearance of Ewing sarcoma at CT is similar to that at radiography, with aggressive bone destruction and a large associated soft-tissue mass (96% of cases) (Figs 2, 3) (53–56). The soft-tissue component is commonly homogeneous and similar in attenuation to that of muscle (98% of cases) (54,56,57). The soft-tissue mass is frequently circumferential but asymmetric about the osseous involvement (Fig 3). Large areas of focal cortical destruction and continuity between the intraosseous and soft-tissue components are common (53% of cases) (Figs 1, 4) (18,36).

However, subtle cortical involvement—which allows communication between the intraosseous and soft-tissue components, appears as lower-attenuation linear channels extending through the high-attenuation cortex, and represents tumor extending along neurovascular channels and haversian canals—is also common (66% of cases) (Fig 1) (18,36). This pattern of intracortical involvement is often subtle at CT, may require viewing at wide window settings, and is the only evidence of cortical destruction in 30% of cases (18,36). In 17% of cases, the cortex appears intact at CT without apparent connection between the medullary canal and soft-tissue components (Figs 2, 3) (18,36). Contrast enhancement is common at CT and is usually either diffuse or peripheral nodular, in our experience (18,36).

Owing to its superior contrast resolution, MR imaging is the optimal radiologic modality in evaluation of bone and soft-tissue tumors, including Ewing sarcoma. MR imaging of Ewing sarcoma of bone reveals marrow replacement (100%) and cortical destruction (92%), with an associated soft-tissue mass in 96% of cases (Figs 2, 3) (18,34,36,58–62). The soft-tissue mass is commonly circumferential but asymmetric about the osseous involvement (Figs 2, 3).

Teaching Point

The signal intensity is usually homogeneous (73%) and intermediate (95%) on T1-weighted images (18,35,36). On T2-weighted images, Ewing sarcoma is typically homogeneous (86%) and low to intermediate in signal intensity (68%) (Figs 2, 3) (18,35,36). This signal intensity and homogeneity are likely related to the high degree of cellularity in Ewing sarcoma. Heterogeneity is seen in 27% of cases on T1-weighted images and 14% on T2-weighted images (18,36). High signal intensity predominates in 32% of Ewing sarcomas of bone on T2-weighted images (36). Heterogeneity and high signal intensity on long TR images are more common in larger lesions and represent hemorrhage or necrosis, in our experience (36). Fluid levels may also be seen as a result of hemorrhage, although this is more common after treatment.

Large areas of focal cortical destruction and continuity between the medullary and soft-tissue components are common at MR imaging (50% of cases) (Fig 4) (18,35,36). However, as at CT, subtle cortical involvement—with linear intermediate signal intensity channels that extend through the low signal intensity cortex, represent tumor extending along the haversian canals and neurovascular channels, and allow connection between the medullary canal and soft-tissue component—is also frequent (Figs 2, 3) (74% of cases) (18,36). This pattern may be the only evidence of cortical involvement and destruction in 40% of cases at MR imaging (36). In our opinion, this pattern of cortical involvement and destruction at either CT or MR imaging, while not specific, strongly suggests a small round blue cell tumor such as Ewing sarcoma or lymphoma or leukemia. In 4% of cases, the cortex between the medullary canal and soft-tissue components appears intact at MR imaging (36). Subperiosteal Ewing sarcoma shows a soft-tissue mass beneath the periosteum without involvement of the medullary canal at CT or MR imaging (Fig 7) (34,38,63–65).

Contrast enhancement is seen in all cases at MR imaging of Ewing sarcoma and is usually either diffuse or peripheral nodular in pattern, in our experience (Figs 2, 3) (18,35,36). Neurovascular and joint involvement by the soft-tissue component is not uncommon. Although patients may present clinically with inflammatory symptoms, edema surrounding Ewing sarcoma at MR imaging is unusual before treatment, unless there is an associated pathologic fracture.

Extraskeletal Ewing Sarcoma

Historically, Ewing sarcoma of soft tissue has included extraskeletal Ewing sarcoma and soft-tissue PNET (6,9–11). In addition, extraskeletal Ewing sarcoma of the thoracopulmonary region is often referred to as Askin tumor (5,6,9–11). Tefft and coworkers (66) described extraskeletal Ewing sarcoma in 1969 and reported four patients with paravertebral soft-tissue tumors that histologically resembled Ewing sarcoma.

As with osseous lesions, soft-tissue PNET and Askin tumor were previously considered to be distinct tumors from extraskeletal Ewing sarcoma. However, just as with Ewing sarcoma of bone, multiple studies support chromosomal and histologic similarities with lack of differentiation, and these lesions (extraskeletal Ewing sarcoma, soft-tissue PNET, and Askin tumor) are also now considered to be in the Ewing sarcoma family of tumors (2,6,9–11,67). These lesions are sarcomas likely of neuroectodermal origin that share the same cytogenetic marker, with translocation of chromosomes t(11;22)(q24;q12) (5,60,68–70). The pathologic appearance is identical to that described earlier for Ewing sarcoma of bone.

Extraskeletal Ewing sarcoma is rare in comparison with Ewing sarcoma of bone (71). The prevalence of extraskeletal Ewing sarcoma is generally accepted to be between 15% and 20% of that of Ewing sarcoma of bone (60,70). PNET has also been rarely reported in a previous site of irradiation (72).

Extraskeletal Ewing sarcoma usually manifests in young patients, with 85% of cases detected between 20 months and 30 years of age (70). However, historically and as with osseous lesions, in soft-tissue PNET the age range has been reported to be wider, from 1 month to 81 years (6,9–11,72). The age range was 20 months to 63 years in Angervall and Enzinger's (2) evaluation of 39 patients. The median age of onset was 20 years in that study (2). As with osseous lesions, extraskeletal Ewing sarcoma is rare in the black population (2,15).

Clinically, patients often have a large, rapidly growing, solitary, superficial or deep soft-tissue mass measuring 5–10 cm at initial presentation (2,73). In Angervall and Enzinger's (2) series of 39 patients, 92% of lesions were deep seated and only 8% were subcutaneous. Pain or tenderness has been reported in 49% of patients (2). The most commonly reported locations of extraskeletal Ewing sarcoma include the paravertebral region (32%), lower extremities (26%), chest wall (18%), retroperitoneum (11%), pelvis and hip (11%), and upper extremities (3%) (2,67,73–75).

Paravertebral masses can manifest as an intradural extramedullary or extradural mass (75). The most common clinical symptoms at presentation for paravertebral extraskeletal Ewing sarcoma include back pain, radicular pain, lower extremity paresis, sensory disturbances, and

bladder or bowel dysfunction (75). Patients with a paravertebral mass at presentation can have symptoms of cord compression due to epidural space involvement, scoliosis, and extremity weakness (2,66,73). Tests for urine catecholamine metabolites are generally negative, unlike in extraadrenal neuroblastoma (5,68) which can also be in the differential diagnosis for a paraspinal mass. Cervical masses can be large enough to cause mass effect on the airway and displacement of the adjacent vasculature (73).

Extraskeletal Ewing sarcoma has been reported to show some differences in comparison with Ewing sarcoma of bone, including the following: *(a)* it does not show as distinct a predilection for male patients, but is more equally distributed between the sexes (although several studies have shown that male patients may be slightly more commonly affected); *(b)* patients are often slightly older (averaging around 20 years of age) by approximately 5–10 years; and *(c)* it more commonly affects the trunk rather than the lower limbs (2,15,73,76).

The following criteria are proposed for the diagnosis of extraskeletal Ewing sarcoma: *(a)* no osseous involvement at MR imaging; *(b)* no increased uptake in bone or periosteum adjacent to the tumor on static images from bone scintigraphy; *(c)* a lesion composed histologically of small round blue tumor cells with no differentiating features at light microscopy, immunohistochemical analysis, or electron microscopy; and *(d)* demonstration of cytoplasmic glycogen (70,71). Meister and Gokel (76) reported three cases of extraskeletal Ewing sarcoma with the lesion located adjacent to the periosteum and with the presence of extrinsic bone erosion or periosteal reaction, but with no evidence of the tumor involving the marrow space.

Overall, imaging features of extraskeletal Ewing sarcoma are nonspecific. At radiography, extraskeletal Ewing sarcoma may manifest as a large soft-tissue mass (50% of cases) or demonstrate a normal appearance. Adjacent bone erosion, cortical thickening, osseous invasion, or aggressive periosteal reaction may also be present (25%–42% of cases) (2,74,77). Similarly, lesion calcification may be identified in up to 25% of cases (2,74,77). Paravertebral masses can cause extrinsic bone erosion and secondary bone reaction in the adjacent vertebral body (66). At angiography, lesions are typically hypervascular.

Nuclear medicine studies including bone scintigraphy and FDG PET typically reveal increased radionuclide uptake in extraskeletal Ewing sarcoma (49,74,78,79). However, as with Ewing sarcoma of bone, photopenia has also been reported rarely (80). At bone scintigraphy, increased radionuclide activity is typically more prominent on the blood flow and blood pool images than on the delayed static images. FDG PET is also useful for detection of the primary lesion as well as residual or recurrent tumor and metastases to the lung or pleura, bone, liver, or soft tissue (49,78–80). Gyorke and colleagues (49) also reported that FDG PET is superior to bone scintigraphy in detection of bone metastases in Ewing sarcoma, although it is inferior to CT in detection of pulmonary metastases owing to the small size of pulmonary nodules.

At ultrasonography (US), O'Keeffe and colleagues (57) reported that extraskeletal Ewing sarcoma lesions are most frequently hypoechoic. Anechoic areas may also be present, likely representing hemorrhage or necrosis (57,77). Increased Doppler blood flow is also present in extraskeletal Ewing sarcoma, in our experience (77).

CT demonstrates a nonspecific soft-tissue mass, most commonly of similar attenuation to that of muscle (87% of cases) (57,77). Low attenuation may also be seen, likely corresponding to areas of hemorrhage or necrosis (57,77). Lesion margins are often poorly defined at CT (60% of cases), which is likely a reflection of the more limited contrast resolution of CT in comparison with that of MR imaging (77). Calcification is seen in 25%–30% of cases (77). Osseous involvement of the bone surface with cortical erosion or periosteal reaction is seen in 40% of cases (77). However, the medullary cavity retains its normal fatty marrow attenuation, a finding reflecting lack of involvement (57,77).

MR imaging features are also nonspecific in evaluation of extraskeletal Ewing sarcoma (Fig 8). MR imaging demonstrates a soft-tissue mass with heterogeneous signal intensity (91%) similar to that of skeletal muscle on T1-weighted images and intermediate to high signal intensity on

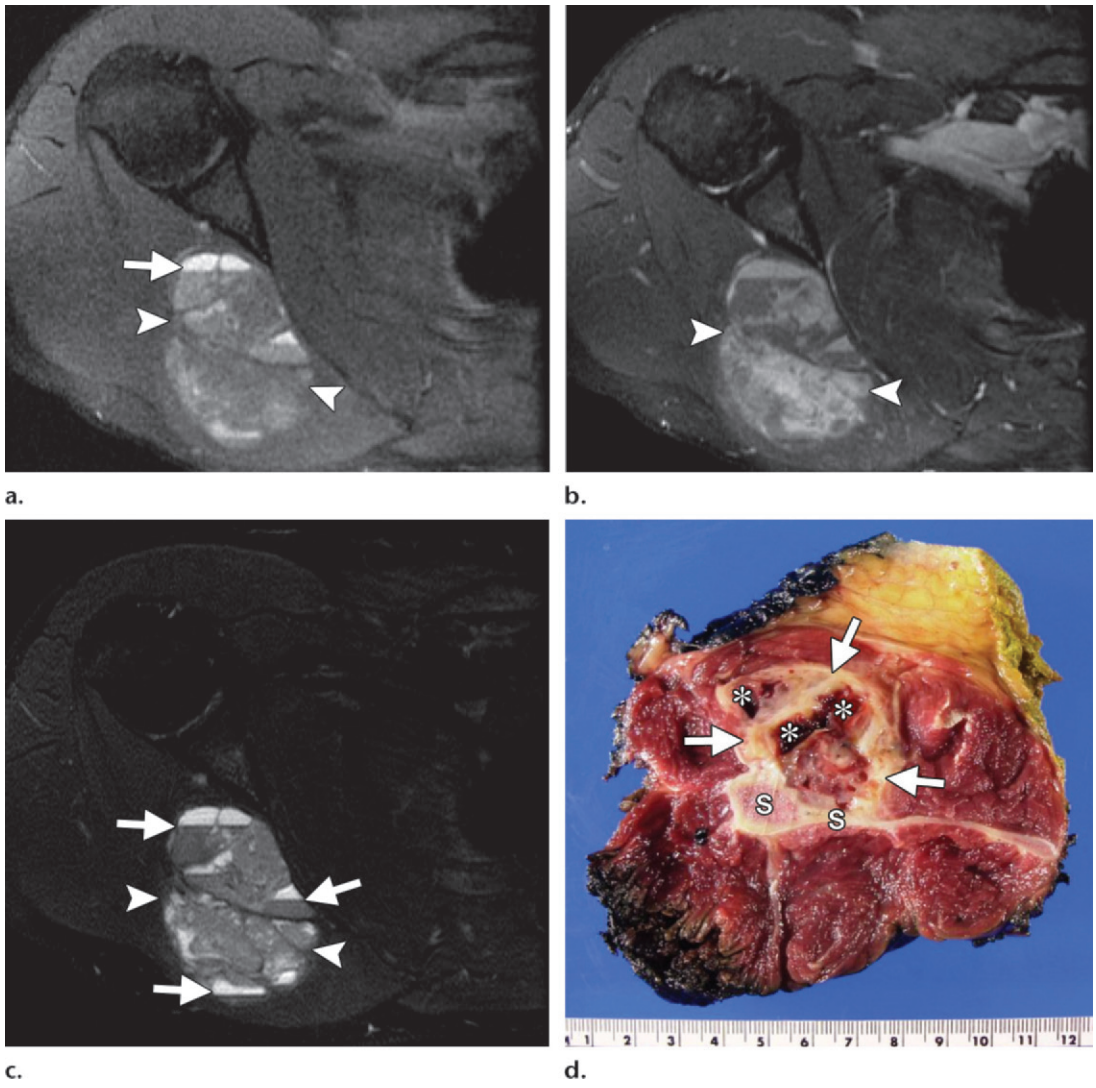

Figure 8. Extraskeletal Ewing sarcoma in a periscapular location in a 21-year-old man with an enlarging painless mass. **(a–c)** Axial precontrast fat-suppressed T1-weighted (600/25) **(a)**, postcontrast fat-suppressed T1-weighted (600/30) **(b)**, and fat-suppressed T2-weighted (4100/60) **(c)** MR images show a periscapular soft-tissue mass (arrowheads). There are multiple fluid levels (arrows in **a** and **c**) that represent hemorrhage, resulting in predominantly heterogeneous intermediate signal intensity with all pulse sequences and diffuse heterogeneous enhancement. No osseous involvement is seen. **(d)** Photograph of the axially sectioned gross specimen demonstrates the periscapular mass (arrows) with hemorrhagic areas (*) adjacent to the scapula *(S)* but without osseous involvement. Scale is in centimeters.

T2-weighted images in 100% of cases (Fig 9) (77). High signal intensity on long TR images predominates in 64% of cases (Fig 9) (77). Intermediate-signal-intensity areas seen on long TR images are likely due to a high degree of cellularity, as in osseous lesions. Areas of hemorrhage appear as high signal intensity on all pulse sequences and are not uncommon; fluid levels may also be evident (Fig 8). Focal areas of necrosis with low signal intensity on T1-weighted images and high signal intensity on T2-weighted images are also frequent (77). As in other soft-tissue masses, MR imaging is also useful for tumor staging and to evaluate the extent of involvement of surrounding structures (73).

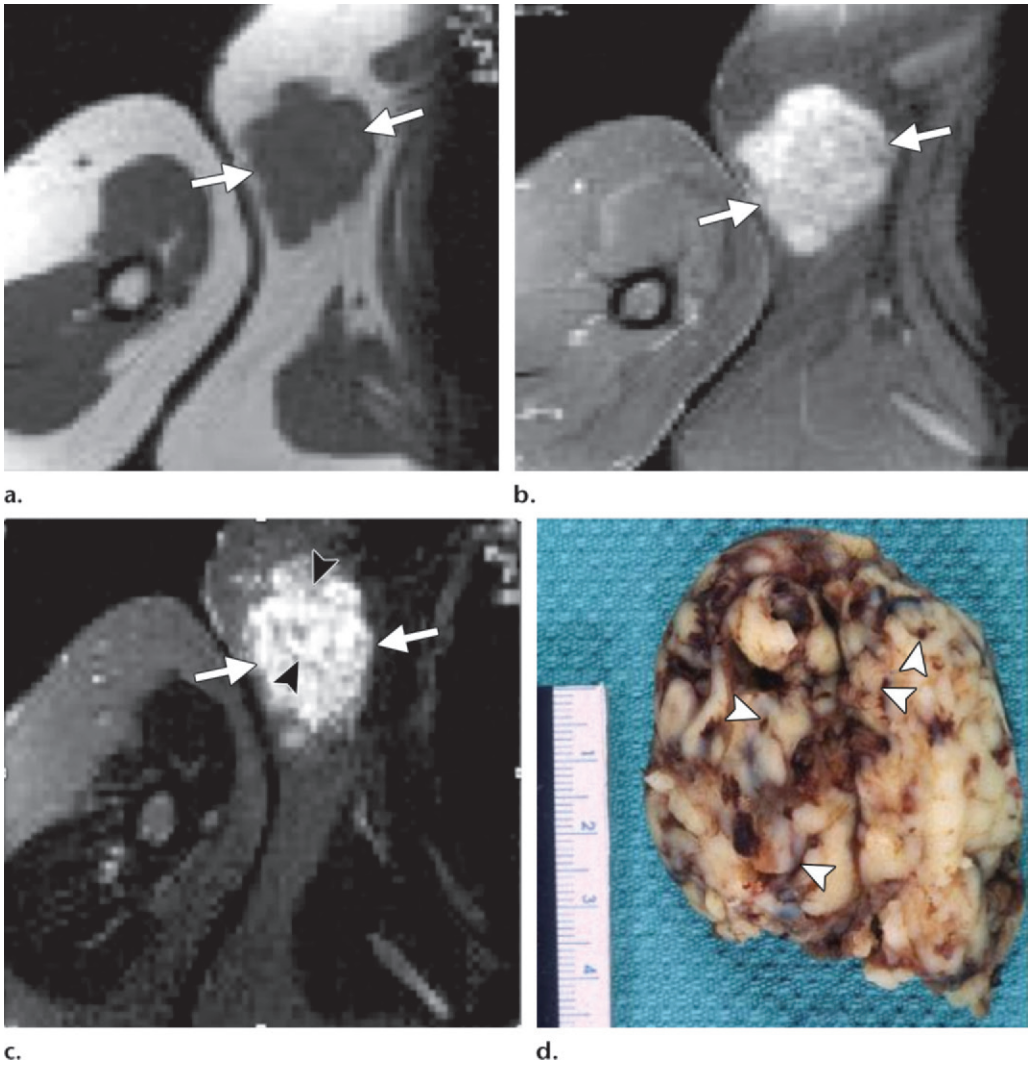

Figure 9. Extraskeletal Ewing sarcoma in an 11-year-old boy with an enlarging axillary soft-tissue mass. **(a–c)** Axial T1-weighted (500/30) **(a)**, postcontrast fat-suppressed T1-weighted (600/25) **(b)**, and T2-weighted (2500/90) **(c)** MR images show a soft-tissue mass (arrows) in the axillary subcutaneous tissue. It has intermediate signal intensity on the T1-weighted image and high signal intensity on the T2-weighted image. Serpentine areas of low signal intensity on the T2-weighted image (arrowheads in **c**) suggest a high-flow vessel component. There is prominent diffuse enhancement after administration of intravenous contrast material. **(d)** Photograph of the sectioned gross specimen demonstrates several prominent intrinsic vascular channels (arrowheads), findings that correspond to the imaging appearance. Scale is in centimeters.

An additional imaging feature that we have recognized at MR imaging of extraskeletal Ewing sarcoma is the presence of serpentine high-flow vascular channels, which have low signal intensity with all pulse sequences in 90% of cases (Fig 9) (77). This finding is not unique to extraskeletal Ewing sarcoma and can be seen in higher-grade vascular lesions (hemangioendothelioma, hemangiopericytoma, and angiosarcoma), rhabdomyosarcoma, synovial sarcoma, and alveolar soft-part sarcoma. However, the presence of this feature in a young person with a large intramuscular mass should raise the possibility of extraskeletal Ewing sarcoma (77).

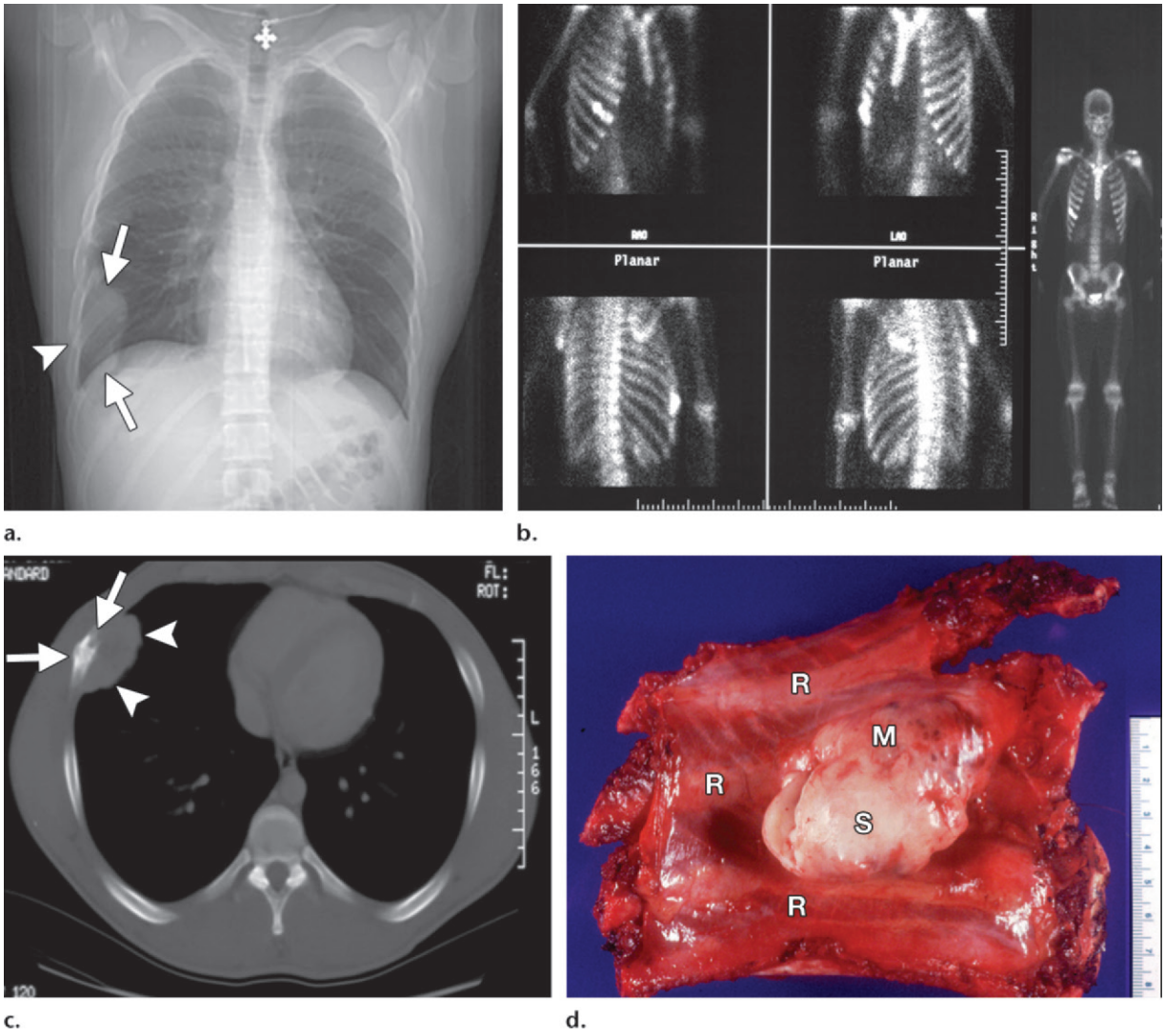

Figure 10. Askin tumor in a 20-year-old man with right lower rib pain and mild tenderness. **(a)** Frontal scout image from CT shows a well-circumscribed mass at the right costophrenic angle (arrows) and subtle bone destruction (arrowhead). **(b)** Images from bone scintigraphy show intense uptake at the right seventh rib. *LAO* = left anterior oblique, *RAO* = right anterior oblique. **(c)** Axial CT image (bone window) reveals a well-circumscribed pleural-based mass (arrowheads) with adjacent bone destruction and periosteal reaction (arrows). **(d)** Photograph of the gross specimen demonstrates three ribs *(R)* with involvement *(M)* of one rib and an associated pleural-based soft-tissue mass *(S)*, findings that correspond to the imaging appearance. Scale is in centimeters.

As with other soft-tissue masses, both benign and malignant, a pseudocapsule with relatively well-defined margins may be seen at MR imaging of extraskeletal Ewing sarcoma (36% of cases) (77). An infiltrative pattern of growth with ill-defined margins is seen at MR imaging in 45% of cases, and neurovascular involvement is seen in 73% (77). Direct invasion of bone is more common in the terminal stage of the disease (2,73). Prominent contrast enhancement is seen at both CT and MR imaging (77).

Askin Tumor

Extraskeletal Ewing sarcoma or PNET located in the thoracopulmonary region is often referred to as Askin tumor (81). In 1979, Askin and coworkers (5) described a malignant small round blue cell tumor in the thoracopulmonary region. This tumor is now believed to develop from embryonal migrating cells of the neural crest (81).

This rare malignant neoplasm is usually seen in young adults and children and typically manifests as a large tumor involving the chest wall and pleura (81). The patients in the study of Askin et al (5) consisted of 20 young children

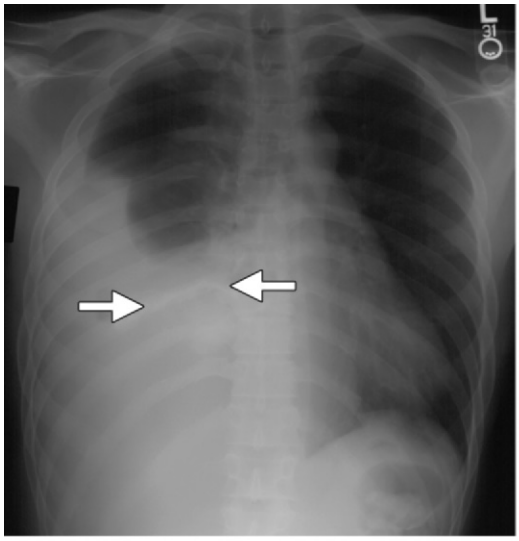

a.

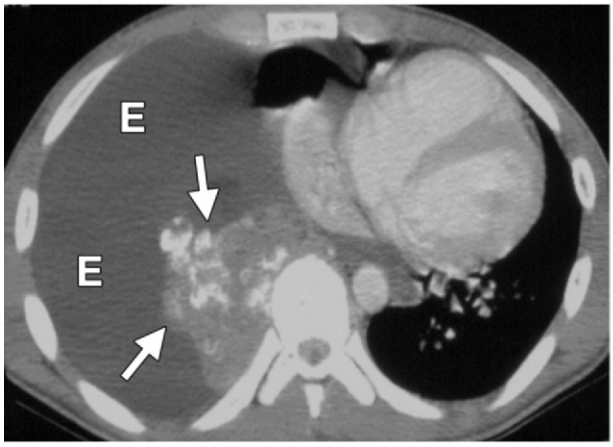

b.

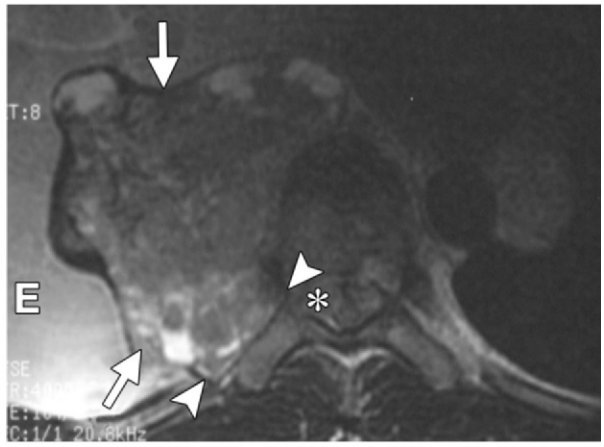

c.

Figure 11. Large Askin tumor of the chest wall in a 26-year-old man with lower back pain and difficulty walking. **(a)** Chest radiograph shows a large mass in the lower right hemithorax, a large pleural effusion, and subtle bone destruction of the posterior ninth rib (arrows). **(b)** Axial CT image (soft-tissue window) reveals a large paravertebral mass with internal coarse calcifications (arrows) and a large pleural effusion *(E)*, which displaces the heart and right lung to the left. **(c)** Axial T2-weighted MR image (4025/16) of the thoracic spine shows a paraspinal mass (arrows) of heterogeneous predominantly low to intermediate signal intensity with a large pleural effusion *(E)* and intradural extension (*), which effaces the cerebrospinal fluid space and causes mass effect on the spinal cord and rib destruction (arrowheads).

and adolescents; their age range at diagnosis was 4 months to 20 years, with a mean of 14.5 years and median of 11 years. A large, unilateral, pleural-based mass with or without pain is the most common clinical presentation (5,68) and was reported in all patients in the study of Winer-Muram and colleagues (81). Patients can also present with constitutional symptoms such as fever, anorexia, and weight loss (82). In contradistinction to osseous Ewing sarcoma, Askin tumor is more commonly seen in female patients (75% of cases) (5,81).

At radiography, a large chest mass is a common finding and represents a combination of a pleural-based mass and pleural fluid (Figs 10, 11) (66,68,82). The associated pleural effusion is often large; it can be loculated and form a pseudotumor (81,82). Pulmonary parenchymal disease may also be apparent in 25% of cases (5). Calcification is uncommon and is seen in only 10% of cases (Fig 11) (5). Ipsilateral hilar and mediastinal adenopathy and pneumothorax are other associated findings (5,68,82).

Rib destruction is frequently associated with Askin tumor (63% of cases) and is associated with increased activity at bone scintigraphy (Fig 10) (68,81,82). A recent case report of Askin tumor demonstrated avid uptake with indium 111 (^{111}In) pentetreotide and technetium 99m (^{99m}Tc) sestamibi (MIBI); however, no uptake was seen at FDG PET (83). Subsequent ^{99m}Tc-MIBI and ^{111}In-pentetreotide scans after surgical resection and chemotherapy were negative, suggesting possible use of these radiopharmaceuticals for follow-up imaging of treatment response (83).

CT often demonstrates a large unilateral chest wall mass with heterogeneous attenuation, which is frequently associated with rib destruction and

pleural effusions (Fig 11) (81). Tumors often have both intrathoracic and extrathoracic components with pleural, pericardial, diaphragmatic, and vertebral or spinal extension and involvement (Fig 11) (81,82).

MR imaging often reveals a large heterogeneous mass with predominantly intermediate signal intensity on T1-weighted images and high signal intensity on T2-weighted images (Fig 11) (81). Prominent areas of high signal intensity compared with that of muscle on both T1- and T2-weighted images are also frequent and represent hemorrhage or necrosis. Direct invasion of the chest wall musculature, mediastinum, or lung is also common (81). Pulmonary involvement can lead to lung collapse (81). Prominent vascular enhancement after intravenous contrast material administration is often demonstrated and reflects tumor hypervascularity (81).

Treatment and Prognosis

Multidisciplinary management is the mainstay of successful treatment of Ewing sarcoma involving bone or soft tissue. After biopsy to confirm the diagnosis, therapy primarily involves initial use of neoadjuvant chemotherapy for the purpose of eliminating micrometastases and reducing the size of the primary tumor. Reducing the size of the primary tumor improves local control, which includes surgical resection, radiation therapy (RT), or both.

Teaching Point

Chemotherapeutic treatment of Ewing sarcoma includes neoadjuvant (before local control) and adjuvant (after local control) therapy over approximately 6 months to 1 year (14). Chemotherapeutic agents commonly used in treatment of Ewing sarcoma include vincristine, doxorubicin, and cyclophosphamide alternated with ifosfamide and etoposide (14,20,84–86). Although specific protocols vary, neoadjuvant chemotherapy is typically given in four to eight cycles in 3-week intervals (85). Future treatment will likely employ molecular therapeutics directed by the cytogenetic aberrations in the Ewing sarcoma family of tumors (87,88).

Surgical treatment of the Ewing sarcoma family of tumors is often the primary method of local control. The goal of surgical resection is to maximize local control and prevent late recurrence resulting from small islands of chemotherapy-resistant cells (89). An additional advantage of surgery is the ability to assess the degree of tumor necrosis in response to neoadjuvant chemotherapy. However, this laudable goal must be balanced with the need to maintain maximum function and limit local mechanical failure.

Factors that should be considered to determine whether surgery can be performed for local control are primarily those of lesion staging. These include patient age; tumor location; tumor extent, size, and volume; involvement of vital soft tissues; relationship to the neurovascular bundle; and whether the tumor can be removed completely with acceptable margins, particularly in expendable and reconstructable locations (14,35). Advances in techniques that preserve or restore limb function (limb salvage techniques) have now made this the preferred surgical treatment for Ewing sarcoma as opposed to amputation, which was commonly employed in the past.

In general, survival rates with limb salvage techniques have been shown to be the same as with amputation, but with the benefit of improved functional outcome and an acceptable risk of complications. Amputation may be necessary in situations where limb salvage procedures are not feasible, including involvement of vital structures by the primary tumor, very large lesions, patients who have not responded to chemotherapy, lesions in the extremities such as the ankle or foot, and cases of a complicated or displaced pathologic fracture (14,90,91).

Surgical treatment as the primary therapy for local control requires complete resection with wide or radical margins to optimize outcome. Wide margins contain normal tissue within the plane of dissection, and the tumor and pseudocapsule are both entirely resected. Radical margins excise all compartments that contain tumor en bloc. In bone, negative margins are defined as having at least a 1-cm rim of surrounding normal tissue, although 2–5-cm margins are recommended (14,35,85,88,92–97). In soft tissue, at least 5 mm of fat or muscle is required for negative margins, with 2 mm through fascial planes and the margins being through noninflamed tissue.

The importance of lesion margin was demonstrated in the study by Sluga and colleagues (92), which revealed that overall survival at 5 years was 60% for wide or radical resection versus 40% for intralesional or marginal resection. Other studies show that this is true only in centrally located tumors; with extremity tumors, no statistically significant difference in local recurrence rates was seen between patients with adequate surgical margins and those with inadequate margins (8% and 10%, respectively) (97). The highest rates of

inadequate surgical margins are associated with central tumors occurring in the scapula (75%), pelvis or sacrum (60%), and ribs (44%) (97).

There are numerous limb salvage surgical resection options available for resection of Ewing sarcoma. The specific reconstruction technique is beyond the scope of this article but is largely dependent on lesion location and stage. These limb salvage options include use of a vascularized bone graft, primary resection of a diaphyseal lesion with segmental sterilization by radiation followed by reimplantation, intercalary allograft, endoprosthetic reconstruction, rotationplasty, expandable prosthesis, or a combination of these techniques (35,88,90).

The surgical treatment of both skeletal and extraskeletal Ewing sarcoma is generally similar. Lee and coworkers (96) found that when both groups of patients were treated with the same protocol, including local control measures with surgery, RT, or both, the outcomes were comparable. Pradhan and colleagues (98) reported similar findings, with no difference in overall survival between patients with skeletal and patients with extraskeletal Ewing sarcoma (64% and 61%, respectively) when the same treatment approach was used. Oncologic outcomes were determined primarily by tumor characteristics rather than the site of origin.

Surgical resection combined with chemotherapy is often the treatment of choice for Ewing sarcoma amenable to a wide excision margin. RT is frequently used to promote improved local control in lesions that are not resectable, in cases with inadequate surgical margins, or in patients with a poor response to chemotherapy (14,98). A preoperative RT dose of 55–60 Gy with a 2–3-cm margin beyond the affected tissue is typically employed (93,98–102). Complications of RT including limb length discrepancy, joint contracture, muscle atrophy, pathologic fracture, and radiation-induced sarcoma have been reported in up to 63% of patients and are more prominent in skeletally immature patients (14,103).

In anatomic sites that are not readily amenable to surgical resection without extensive morbidity (pelvis and axial skeleton), chemotherapy and RT without surgery may be employed in the treatment of Ewing sarcoma. These lesions have a higher prevalence of concomitant metastatic disease and lower survival rates (40% at 5 years vs as high as 85% at 5 years for extremity tumors) in some studies (14,89,100,104,105). In general, many studies have shown improved local control and survival with surgery and chemotherapy (with or without RT) versus RT and chemotherapy alone (25% vs 15% 5-year survival and 5%–10% vs 35% local recurrence rate, respectively) (14,104,105).

These aggressive therapies have resulted in an overall improved 5-year survival from 63% to 82% in patients with localized disease and from 25% to 39% in patients with metastatic disease at clinical presentation (14,85,100,106–112). Unfortunately, 15%–30% of patients with Ewing sarcoma demonstrate metastatic disease at presentation (9,14,111), most commonly affecting bone, the liver, or the lung (14,113,114). Metastasis to the lung (12%–36% alone at presentation) or bone (7%–37% alone at presentation) has been reported in 18%–41% of patients at presentation (21% have both bone and lung involvement) (14,17,35,45,111,115–117). The most frequent sites of osseous metastatic disease in Ewing sarcoma are the pelvis (26%), femur (20%), tibia or fibula (18%), chest wall (16%), upper extremity (9%), and spine (6%) (48,85).

These patients reveal a significantly worsened prognosis, although Miser and colleagues (118) reported an 8-year event-free survival of 20% and cure rate of 14%–28%. The identification of multiple metastases is associated with a worsened prognosis in comparison with the presence of a single metastasis (114). Haeusler and coworkers (113) demonstrated improved event-free survival at 3 years when aggressive local control for extrapulmonary metastases was undertaken, in particular with both surgery and RT (56%) in comparison with either modality alone (34%). Pulmonary metastases are optimally treated with RT versus metastasectomy (14,113,119,120).

The overall prognosis of Askin tumor is poor in comparison with Ewing sarcoma at other sites, with a median survival reported by Askin and coworkers (5) in 1979 of only 8 months. More recent reports show that the prognosis is usually poor, with 2-year and 6-year survival rates of 38% and 14%, respectively (121). Recurrence is seen in more than 50% of cases, manifesting as local disease, mediastinal lymphadenopathy, or pulmonary nodules (66). Recurrent thoracic disease with direct extension into the pleura or lungs and pulmonary nodules is the most common manifestation of initial treatment failure (68). Pulmonary metastasis was seen in 38% of cases of Askin tumor at presentation, and mediastinal lymphadenopathy was seen in 25% (81).

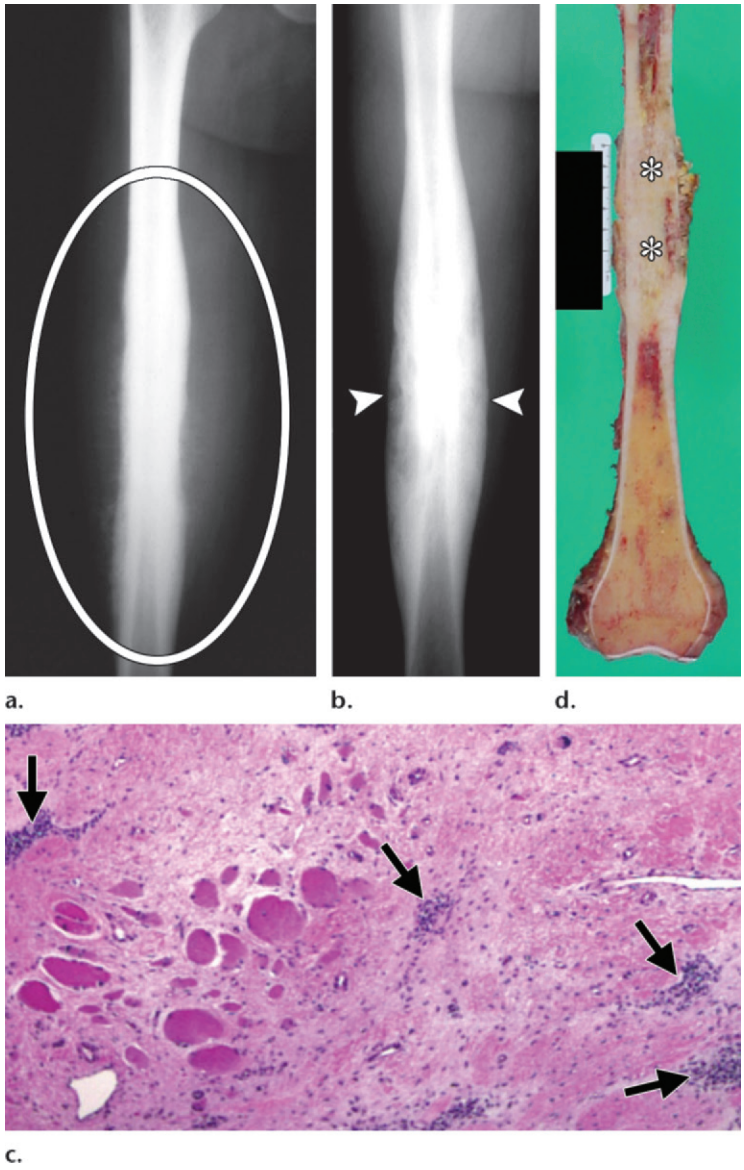

Figure 12. Radiographic response to treatment in a 21-year-old man. **(a)** Frontal radiograph at initial diagnosis shows a permeative lytic bone lesion in the mid diaphysis of the femur and hair-on-end periosteal reaction (white oval). **(b)** Frontal radiograph of the femur 6 months after chemotherapy and RT reveals increased sclerosis and maturation of periosteal reaction (arrowheads), findings that represent a favorable response to therapy. **(c)** Photomicrograph (original magnification, ×250; H-E stain) shows extensive necrosis of tumor (red areas) with only small foci of viable blue tumor cells (arrows). **(d)** Photograph of the coronally sectioned gross specimen demonstrates similar findings of sclerosis (∗). Scale is in centimeters.

CT is the superior modality for diagnosis of pulmonary metastasis and local recurrence (81). Osteoblastic bone metastasis is seen in approximately 25% of patients (68). Metastasis to the sympathetic chain has also been reported and may support the neuroectodermal origin of the tumor (68). Hepatic and adrenal metastases have also been rarely described (68).

Local recurrence of Ewing sarcoma typically occurs within 5 years after diagnosis in 85%–90% of cases (14,97). The prognosis in patients with recurrence or progressive disease is poor, with less than 10% survival (14,122). Local recurrence is typically treated with radical resection or amputation.

The risk of secondary malignancy in patients with Ewing sarcoma is also significant, with 1%–2% of survivors developing acute myeloid leukemia or myelodysplastic syndrome (14,123–125). In addition, there is a cumulative risk of 20% (at 20 years) for development of a second bone sarcoma (14,126).

Numerous factors have been associated with a worsened prognosis in patients with the Ewing sarcoma family of tumors. These include tumor size greater than 8 cm at presentation, central location (pelvis), older patient age, type of cytogenetic aberration, increased level of serum lactate dehydrogenase, metastatic disease at presentation, recurrence within 2 years, and—perhaps most important—less than 90% necrosis with neoadjuvant chemotherapy (14,94,105,127,128).

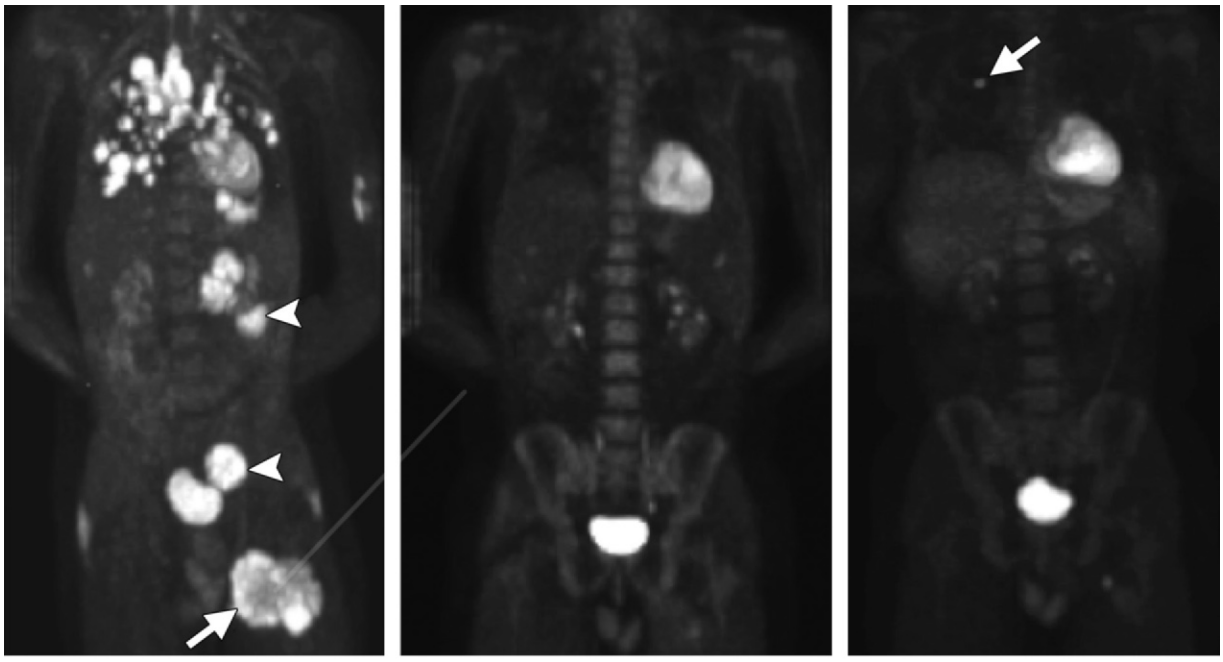

a. b. c.

Figure 13. Extraskeletal Ewing sarcoma involving the left thigh in a 22-year-old man. **(a)** Maximum intensity projection (MIP) image from staging whole-body FDG PET demonstrates a dominant left thigh mass (arrow) with widespread metastases to lymph nodes (arrowheads) and the lungs. **(b)** Follow-up MIP image from restaging whole-body FDG PET after 1.5 months of chemotherapy reveals a marked decrease in hypermetabolic activity at both the primary and metastatic sites. **(c)** MIP image from restaging whole-body FDG PET 4.5 months after initiation of therapy reveals a new right pulmonary metastasis (arrow) despite continuation of therapy. The patient died approximately 2 months later.

Posttreatment Imaging

Imaging after institution of neoadjuvant therapy (chemotherapy, RT, or both) is important to evaluate response to treatment. At radiography, common findings that are associated with a favorable response to therapy of osseous Ewing sarcoma at the tumor primary site include maturation of periosteal reaction, coarsening of the bone trabeculae, reconstitution of the cortex, increasing osseous sclerosis and progressive mineralization, and decrease in the size of the soft-tissue component of the lesion (Fig 12) (9,18,129). These features of healing are typically complete by approximately 1 year after initiation of treatment, although reconstitution of the cortex may continue for 2 years (18,129,130). Unfortunately, these radiographic features of a favorable response to neoadjuvant therapy cannot be quantitated as to degree of tumor necrosis or used to predict treatment outcome.

In contradistinction, absence of these radiographic findings of healing and presence of increasing bone destruction after treatment of osseous Ewing sarcoma suggest lack of a favorable response to neoadjuvant therapy and tumor progression (18,130). Lytic areas that are more widely distributed may be seen with radiation osteitis (18). Osseous metastases may be lytic, sclerotic, or mixed at radiography. Skip metastasis, tumor in the same bone as the primary lesion but separated from it by normal intervening marrow, has been reported in 4%–6% of Ewing sarcomas (116). Evaluation of skip metastases requires assessment of the entire long bone at the primary site with MR imaging, bone scintigraphy, or FDG PET (Fig 4). Overall, metastases are best evaluated with abdominal CT, bone scintigraphy, FDG PET, or whole-body MR imaging. Daldrup-Link and colleagues (131) found FDG PET (90% sensitivity) superior to bone scintigraphy (82% sensitivity) or whole-body MR imaging (71% sensitivity) in evaluation of bone metastases in children.

Bone scintigraphy may reveal diminishing uptake of radionuclide in response to therapy (15,35). FDG PET is more useful in evaluation of tumor response to treatment, with its ability to depict molecular changes before the morphologic abnormalities evaluated with cross-sectional imaging (Fig 13). The maximum SUV is generally regarded as a reliable marker of

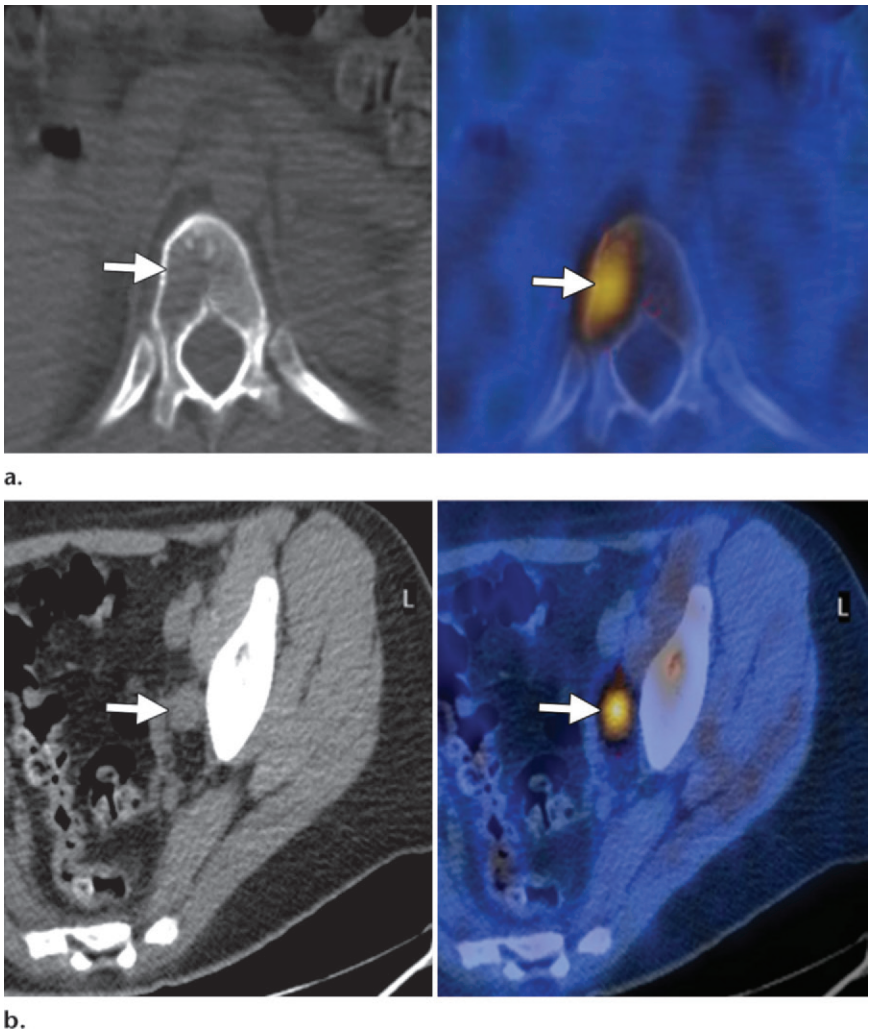

Figure 14. Use of PET/CT for restaging after neoadjuvant chemotherapy in an 18-year-old woman with a history of Askin tumor. **(a)** Left: Restaging axial CT image shows a lytic bone lesion (arrow) in a thoracic vertebral body. Right: Fused PET/CT image demonstrates intense hypermetabolic activity in the lesion (arrow). **(b)** Left: Axial CT image shows a new left pelvic lymph node (arrow). Right: Fused PET/CT image reveals intense hypermetabolic activity in the lymph node (arrow). These findings were proved to represent bone and lymph node metastases at biopsy.

disease activity (48,50). Franzius and colleagues (46) showed that patients with a good response to chemotherapy (>90% necrosis) in primary bone sarcomas had a greater than 30% decrease in tumoral-to-nontumoral activity. Hawkins and colleagues (132) found that a maximum SUV of less than 2.5 after chemotherapy was associated with increased progression-free survival and a positive predictive value for favorable response (<10% viable tumor) of 79% in osseous Ewing sarcoma. Similar features are reported with FDG PET in extraskeletal Ewing sarcoma (Fig 14) (70,133).

FDG PET also demonstrates high accuracy in detection of tumor recurrence locally and distally (Fig 14). Franzius and coworkers (46) reported a sensitivity of 96%, specificity of 81%, and accuracy of 90% in detecting tumor recurrence in a series of 27 primary osseous sarcomas (21 Ewing sarcomas). Similarly, Arush and colleagues (134) showed that in 19 malignant bone and soft-tissue sarcomas (nine Ewing sarcomas), FDG PET helped detect 80% of cases of recurrent disease and was the only modality to demonstrate distant metastases in 15% of the patients (Fig 14). Gaston and colleagues (50) more recently suggested that the metabolic tumor volume (MTV) is a better predictor of treatment response than SUV at FDG PET. In their study, a 90% reduction in MTV was predictive of a good response to chemotherapy for Ewing sarcoma (50).

CT reveals similar osseous features of a favorable response to therapy as discussed earlier for radiography (18,35,62,129). CT is superior to radiography in assessment of the soft-tissue component but inferior to MR imaging. A decrease in the size of the extraosseous component represents a favorable response to treatment (62,135,136). CT findings of a poor response include enlargement of the soft-tissue component, progressive bone destruction, and an increase in the extent of marrow involvement (18,57,129).

Figure 15. Effects of chemotherapy in an 11-year-old boy with Ewing sarcoma of the proximal fibula. **(a)** Axial postcontrast T1-weighted MR image (600/25) shows medullary involvement in the fibular metadiaphysis with a large asymmetric soft-tissue component (*), which is most prominent laterally. **(b)** Axial T2-weighted MR image (3825/40) after 3 months of chemotherapy reveals near-complete resolution of the entire soft-tissue component, with small subperiosteal residua anteromedially (*). **(c)** Photograph of the sectioned gross specimen demonstrates a similar marked reduction in lesion size, with sclerosis (arrows) and a small subperiosteal component (arrowheads). Scale is in centimeters. **(d)** Photomicrograph (original magnification, ×100; H-E stain) shows a largely necrotic tumor (red areas) between trabecular bone *(T)* with small islands of viable tumor (arrows), findings that represent a good response to chemotherapy (>90% necrosis).

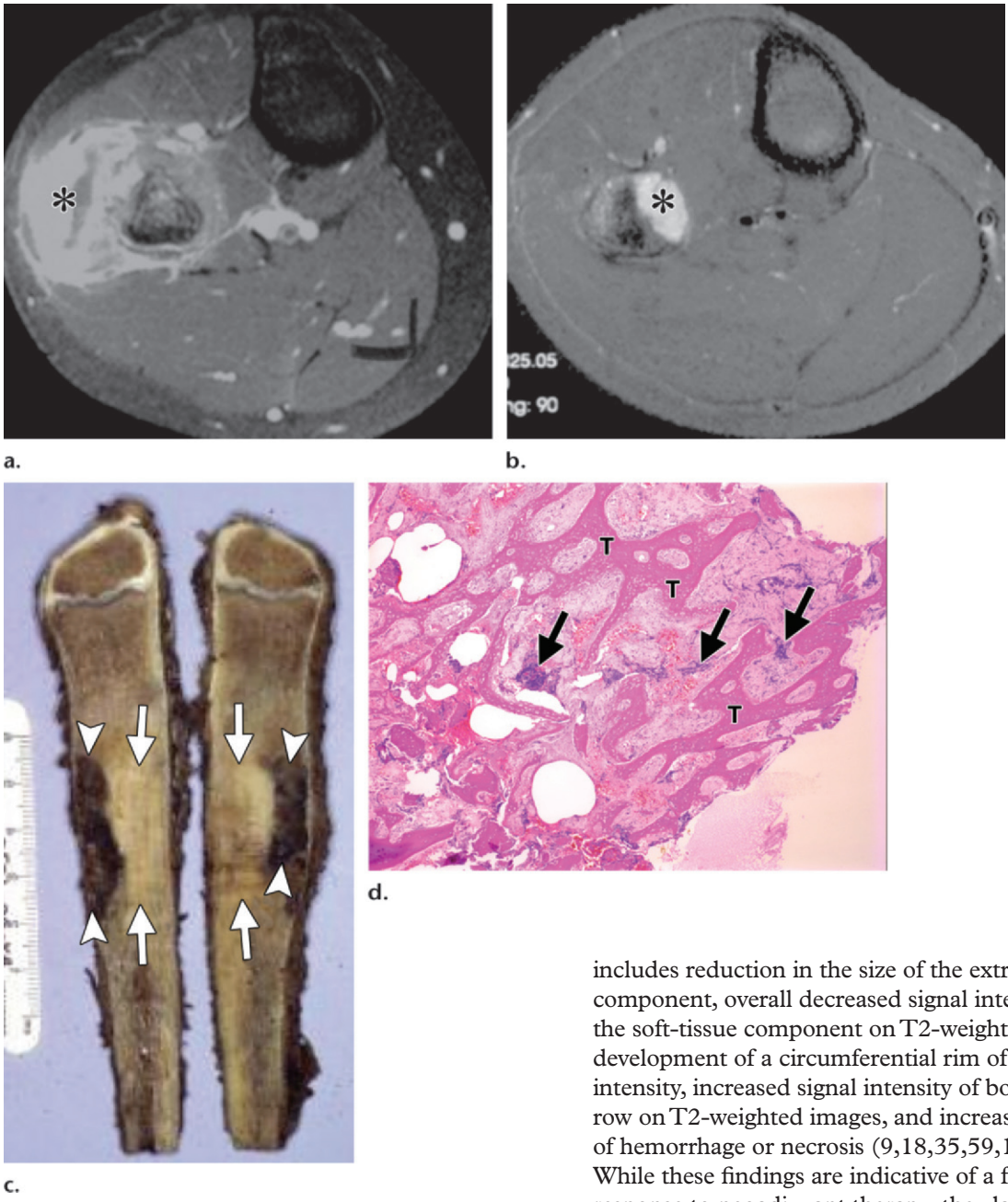

MR imaging is the optimal radiologic modality for assessment of treatment effects in Ewing sarcoma due to its superior contrast resolution (Fig 15). A favorable response to neoadjuvant therapy for both osseous and extraosseous Ewing sarcoma includes reduction in the size of the extraosseous component, overall decreased signal intensity of the soft-tissue component on T2-weighted images, development of a circumferential rim of low signal intensity, increased signal intensity of bone marrow on T2-weighted images, and increasing areas of hemorrhage or necrosis (9,18,35,59,137,138). While these findings are indicative of a favorable response to neoadjuvant therapy, they lack sensitivity for detection of greater than 90% necrosis related to treatment (the definition of a positive response), which is associated with improved long-term survival (Fig 15).

Dynamic contrast-enhanced MR imaging has been used to quantitate the degree of necrosis corresponding to a positive response histologically (9,30,138,139). The general concept of dynamic contrast-enhanced MR imaging in post-therapy imaging is that areas of rapid enhancement (<6 seconds) with a steeper slope on a time-intensity curve represent viable tumor and can be quantitated with regions of interest. This allows quantitative assessment of tumor necrosis. In Ewing sarcoma, a good response (>90% necrosis) is predicted by the presence of only a small cuff of residual enhancement without nodularity at dynamic contrast-enhanced MR imaging (138–140). In contradistinction, a poor response is indicated by a limited reduction in tumor volume (<25%) and enhancing nodules greater than 3 mm in size (138,140).

Doppler US can be used similarly to evaluate response to therapy in Ewing sarcoma but is limited to assessment of the extraosseous component. Increased peripheral resistance and significant decrease in Doppler shift are associated with a good therapy response, whereas decreased peripheral resistance and high-frequency Doppler shifts are characteristic of a poor response (138,139). The potential use of diffusion-weighted MR imaging with apparent diffusion coefficient (ADC) maps has also been described in monitoring small differences in variable chemotherapeutic regimens in Ewing sarcoma (139,141).

Summary

The Ewing sarcoma family of tumors includes Ewing sarcoma of bone, extraskeletal Ewing sarcoma, PNET, and Askin tumor. While these lesions were previously considered distinct neoplasms, the advent of cytogenetic evaluation has allowed identification of a common karyotype abnormality with a translocation involving chromosomes 11 and 22. This shared cytogenetic aberration has led to near-universal agreement that these neoplasms are closely related if not identical, and they are referred to as the Ewing sarcoma family of tumors. Histologically, these lesions demonstrate crowded sheets of small round blue cells.

Imaging features of osseous Ewing sarcoma often suggest the diagnosis. They include the aggressive characteristics of moth-eaten to permeative bone destruction in the metadiaphysis or diaphysis of a long bone in an adolescent or young adult with an associated, often large, soft-tissue mass. Large focal areas of cortical destruction are frequent, allowing continuity between the intraosseous and extraosseous components. However, this continuity is also commonly seen as subtle channels of bone destruction extending through the cortex at CT or MR imaging. This imaging feature suggests a small round blue cell tumor and is a reflection of the underlying pathologic appearance.

Extraskeletal Ewing sarcoma commonly demonstrates a nonspecific radiologic appearance of a large soft-tissue mass affecting the paraspinal region or lower extremity. Detection of high-flow vessels within the lesion at MR imaging, while not specific, is an additional finding suggestive of this diagnosis. Askin tumor represents extraskeletal Ewing sarcoma involving the chest wall. Imaging typically reveals a large pleural-based soft-tissue mass and associated pleural effusion.

Treatment of the Ewing sarcoma family of tumors is usually a combination of neoadjuvant chemotherapy followed by surgical resection, which may be supplemented with RT. Imaging, particularly MR imaging, is also vital to evaluate response to neoadjuvant therapy, direct surgical resection, and detect local recurrence or metastatic disease.

Acknowledgments.—The authors gratefully acknowledge the support of Janice Danqing Liu for manuscript preparation and the residents who attend the AIRP radiologic pathology courses (past, present, and future)—without whom this project would not have been possible—for their contributions to our series of patients.

References

1. Ewing J. Diffuse endothelioma of bone. Proc N Y Pathol Soc 1921;21(1):17–24.
2. Angervall L, Enzinger FM. Extraskeletal neoplasm resembling Ewing's sarcoma. Cancer 1975;36(1):240–251.
3. Seemayer TA, Thelmo WL, Bolande RP, Wiglesworth FW. Peripheral neuroectodermal tumors. Perspect Pediatr Pathol 1975;2:151–172.
4. Jaffe R, Santamaria M, Yunis EJ, et al. The neuroectodermal tumor of bone. Am J Surg Pathol 1984;8(12):885–898.

5. Askin FB, Rosai J, Sibley RK, Dehner LP, McAlister WH. Malignant small cell tumor of the thoracopulmonary region in childhood: a distinctive clinicopathologic entity of uncertain histogenesis. Cancer 1979;43(6):2438–2451.
6. Dorfman HD, Czerniak B. Ewing's sarcoma and related entities. In: Dorfman HD, Czerniak B, eds. Bone tumors. St Louis, Mo: Mosby, 1998; 607–663.
7. Aurias A, Rimbaut C, Buffe D, Zucker JM, Mazabraud A. Translocation involving chromosome 22 in Ewing's sarcoma: a cytogenetic study of four fresh tumors. Cancer Genet Cytogenet 1984;12(1):21–25.
8. Cavazzana AO, Magnani JL, Ross RA, Miser J, Triche TJ. Ewing's sarcoma is an undifferentiated neuroectodermal tumor. Prog Clin Biol Res 1988; 271:487–498.
9. Resnick D, Kyriakos M, Greenway G. Tumors and tumor-like lesions of bone: imaging and pathology of specific lesions. In: Resnick D, Niwayama G, eds. Diagnosis of bone and joint disorders. Philadelphia, Pa: Saunders, 2002; 4060–4073.
10. Unni K. Small cell malignancies. In: Unni K, Inwards C, Bridge J, Kindblom L, Wold L, eds. AFIP atlas of tumor pathology series 4: tumors of the bone and joints. Washington, DC: American Registry of Pathology, 2005; 209–248.
11. Ushigome S, Machinami R, Sorensen P. In: Fletcher D, Krishnan K, Mertens F, eds. Ewing sarcoma/primitive neuroectodermal tumour (PNET). Lyon, France: IARC, 2001; 298–300.
12. Barker LM, Pendergrass TW, Sanders JE, Hawkins DS. Survival after recurrence of Ewing's sarcoma family of tumors. J Clin Oncol 2005;23(19): 4354–4362.
13. Gurney JG, Severson RK, Davis S, Robison LL. Incidence of cancer in children in the United States: sex-, race-, and 1-year age-specific rates by histologic type. Cancer 1995;75(8):2186–2195.
14. Maheshwari AV, Cheng EY. Ewing sarcoma family of tumors. J Am Acad Orthop Surg 2010;18(2): 94–107.
15. Reinus WR, Gilula LA. Radiology of Ewing's sarcoma: Intergroup Ewing's Sarcoma Study (IESS). RadioGraphics 1984;4(6):929–944.
16. Worch J, Matthay KK, Neuhaus J, Goldsby R, DuBois SG. Ethnic and racial differences in patients with Ewing sarcoma. Cancer 2010;116(4):983–988.
17. Pritchard DJ, Dahlin DC, Dauphine RT, Taylor WF, Beabout JW. Ewing's sarcoma: a clinicopathological and statistical analysis of patients surviving five years or longer. J Bone Joint Surg Am 1975;57(1):10–16.
18. Kransdorf MJ, Smith SE. Lesions of unknown histogenesis: Langerhans cell histiocytosis and Ewing sarcoma. Semin Musculoskelet Radiol 2000;4(1): 113–125.
19. Widhe B, Widhe T. Initial symptoms and clinical features in osteosarcoma and Ewing sarcoma. J Bone Joint Surg Am 2000;82(5):667–674.
20. Potratz J, Jürgens H, Craft A, Dirksen U. Ewing sarcoma: biology-based therapeutic perspectives. Pediatr Hematol Oncol 2012;29(1):12–27.
21. Fletcher CDM, Unni KK, Mertens F. Pathology and genetics of tumours of soft tissue and bone. Lyon, France: IARC, 2002.
22. Shirley SK, Gilula LA, Siegal GP, Foulkes MA, Kissane JM, Askin FB. Roentgenographic-pathologic correlation of diffuse sclerosis in Ewing sarcoma of bone. Skeletal Radiol 1984;12(2):69–78.
23. Nascimento AG, Unii KK, Pritchard DJ, Cooper KL, Dahlin DC. A clinicopathologic study of 20 cases of large-cell (atypical) Ewing's sarcoma of bone. Am J Surg Pathol 1980;4(1):29–36.
24. Bridge JA, Fidler ME, Neff JR, et al. Adamantinoma-like Ewing's sarcoma: genomic confirmation, phenotypic drift. Am J Surg Pathol 1999;23(2): 159–165.
25. Schajowicz F. Ewing's sarcoma and reticulum-cell sarcoma of bone; with special reference to the histochemical demonstration of glycogen as an aid to differential diagnosis. J Bone Joint Surg Am 1959;41-A(2):349–356, passim.
26. Fellinger EJ, Garin-Chesa P, Triche TJ, Huvos AG, Rettig WJ. Immunohistochemical analysis of Ewing's sarcoma cell surface antigen p30/32MIC2. Am J Pathol 1991;139(2):317–325.
27. Devaney K, Abbondanzo SL, Shekitka KM, Wolov RB, Sweet DE. MIC2 detection in tumors of bone and adjacent soft tissues. Clin Orthop Relat Res 1995;(310):176–187.
28. Tsokos M, Alaggio RD, Dehner LP, Dickman PS. Ewing sarcoma/peripheral primitive neuroectodermal tumor and related tumors. Pediatr Dev Pathol 2012;15(1 suppl):108–126.
29. Burchill S, Picton S, Wheeldon J, Kinsey S, Lashford L, Lewis I. Reduced tumor load in peripheral blood after treatment with G-CSF and chemotherapy in children with tumors of the Ewing sarcoma family but not neuroblastoma. Blood 2003;102(9): 3459–3460.
30. Fletcher BD, Hanna SL, Fairclough DL, Gronemeyer SA. Pediatric musculoskeletal tumors: use of dynamic, contrast-enhanced MR imaging to monitor response to chemotherapy. Radiology 1992;184 (1):243–248.
31. Kumar S, Pack S, Kumar D, et al. Detection of EWS-FLI-1 fusion in Ewing's sarcoma/peripheral primitive neuroectodermal tumor by fluorescence in situ hybridization using formalin-fixed paraffin-embedded tissue. Hum Pathol 1999;30(3):324–330.
32. Liao DJ, Thakur A, Wu J, Biliran H, Sarkar FH. Perspectives on c-Myc, cyclin D1, and their interaction in cancer formation, progression, and response to chemotherapy. Crit Rev Oncog 2007;13(2):93–158.
33. Eggli KD, Quiogue T, Moser RP Jr. Ewing's sarcoma. Radiol Clin North Am 1993;31(2):325–337.
34. Saifuddin A, Whelan J, Pringle JA, Cannon SR. Malignant round cell tumours of bone: atypical clinical and imaging features. Skeletal Radiol 2000;29(11): 646–651.

35. Mar WA, Taljanovic MS, Bagatell R, et al. Update on imaging and treatment of Ewing sarcoma family tumors: what the radiologist needs to know. J Comput Assist Tomogr 2008;32(1):108–118.
36. Smith SE, Murphey MD, Jelinek JS, Torop AH, Mulligan ME, Flemming DJ. Imaging of Ewing sarcoma and primitive neuroectodermal tumor of bone with pathologic correlation and emphasis on CT and MRI [abstr]. Radiology 1998;209(P):420.
37. Hammoud S, Frassica FJ, McCarthy EF. Ewing's sarcoma presenting as a solitary cyst. Skeletal Radiol 2006;35(7):533–535.
38. Shapeero LG, Vanel D, Sundaram M, et al. Periosteal Ewing sarcoma. Radiology 1994;191(3):825–831.
39. Baraga JJ, Amrami KK, Swee RG, Wold L, Unni KK. Radiographic features of Ewing's sarcoma of the bones of the hands and feet. Skeletal Radiol 2001;30(3):121–126.
40. Grubb MR, Currier BL, Pritchard DJ, Ebersold MJ. Primary Ewing's sarcoma of the spine. Spine 1994;19(3):309–313.
41. Venkateswaran L, Rodriguez-Galindo C, Merchant TE, Poquette CA, Rao BN, Pappo AS. Primary Ewing tumor of the vertebrae: clinical characteristics, prognostic factors, and outcome. Med Pediatr Oncol 2001;37(1):30–35.
42. Ilaslan H, Sundaram M, Unni KK, Dekutoski MB. Primary Ewing's sarcoma of the vertebral column. Skeletal Radiol 2004;33(9):506–513.
43. Jones GR, Miller JH, White L, Laug WE, Shore NA. Improved detection of metastatic Ewing's sarcoma with the use of bone marrow scintigraphy. Med Pediatr Oncol 1987;15(2):78–81.
44. Estes DN, Magill HL, Thompson EI, Hayes FA. Primary Ewing sarcoma: follow-up with Ga-67 scintigraphy. Radiology 1990;177(2):449–453.
45. Hugenholtz EA, Piers DA, Kamps WA, et al. Bone scintigraphy in nonsurgically treated Ewing's sarcoma at diagnosis and follow-up: prognostic information of the primary tumor site. Med Pediatr Oncol 1994;22(4):236–239.
46. Franzius C, Sciuk J, Daldrup-Link HE, Jürgens H, Schober O. FDG-PET for detection of osseous metastases from malignant primary bone tumours: comparison with bone scintigraphy. Eur J Nucl Med 2000;27(9):1305–1311.
47. Gupta H, Grainger AJ. A soft tissue groin mass. Skeletal Radiol 2010;39(7):707, 725–726.
48. Bestic JM, Peterson JJ, Bancroft LW. Pediatric FDG PET/CT: physiologic uptake, normal variants, and benign conditions [corrected]. RadioGraphics 2009; 29(5):1487–1500.
49. Györke T, Zajic T, Lange A, et al. Impact of FDG PET for staging of Ewing sarcomas and primitive neuroectodermal tumours. Nucl Med Commun 2006;27(1):17–24.
50. Gaston LL, Di Bella C, Slavin J, Hicks RJ, Choong PF. 18F-FDG PET response to neoadjuvant chemotherapy for Ewing sarcoma and osteosarcoma are different. Skeletal Radiol 2011;40(8):1007–1015.
51. Treglia G, Salsano M, Stefanelli A, Mattoli MV, Giordano A, Bonomo L. Diagnostic accuracy of 18F-FDG-PET and PET/CT in patients with Ewing sarcoma family tumours: a systematic review and a meta-analysis. Skeletal Radiol 2012;41(3):249–256.
52. Völker T, Denecke T, Steffen I, et al. Positron emission tomography for staging of pediatric sarcoma patients: results of a prospective multicenter trial. J Clin Oncol 2007;25(34):5435–5441.
53. Ginaldi S, deSantos LA. Computed tomography in the evaluation of small round cell tumors of bone. Radiology 1980;134(2):441–446.
54. Vanel D, Contesso G, Couanet D, Piekarski JD, Sarrazin D, Masselot J. Computed tomography in the evaluation of 41 cases of Ewing's sarcoma. Skeletal Radiol 1982;9(1):8–13.
55. Rosenthal DI. Computed tomography of orthopedic neoplasms. Orthop Clin North Am 1985;16(3):461–470.
56. Williams MP, Husband JE, McElwain TJ. Role of computed tomography scanning in the management of Ewing's sarcoma. Med Pediatr Oncol 1989;17(5):414–417.
57. O'Keeffe F, Lorigan JG, Wallace S. Radiological features of extraskeletal Ewing sarcoma. Br J Radiol 1990;63(750):456–460.
58. Frouge C, Vanel D, Coffre C, Couanet D, Contesso G, Sarrazin D. The role of magnetic resonance imaging in the evaluation of Ewing sarcoma: a report of 27 cases. Skeletal Radiol 1988;17(6):387–392.
59. Lemmi MA, Fletcher BD, Marina NM, et al. Use of MR imaging to assess results of chemotherapy for Ewing sarcoma. AJR Am J Roentgenol 1990;155(2):343–346.
60. Parham DM, Hijazi Y, Steinberg SM, et al. Neuroectodermal differentiation in Ewing's sarcoma family of tumors does not predict tumor behavior. Hum Pathol 1999;30(8):911–918.
61. Kauffman WM, Fletcher BD, Hanna SL, Meyer WH. MR imaging findings in recurrent primary osseous Ewing sarcoma. Magn Reson Imaging 1994;12(8):1147–1153.
62. van der Woude HJ, Bloem JL, Hogendoorn PC. Preoperative evaluation and monitoring chemotherapy in patients with high-grade osteogenic and Ewing's sarcoma: review of current imaging modalities. Skeletal Radiol 1998;27(2):57–71.
63. Bator SM, Bauer TW, Marks KE, Norris DG. Periosteal Ewing's sarcoma. Cancer 1986;58(8):1781–1784.
64. Kolár J, Zídková H, Matějovsky Z, Povýsil C, Kolín J, Beran J. Periosteal Ewing's sarcoma. Rofo 1989;150(2):179–182.

65. Wuisman P, Roessner A, Blasius S, Erlemann R, Winkelmann W, Ritter J. (Sub)periosteal Ewing's sarcoma of bone. J Cancer Res Clin Oncol 1992; 118(1):72–74.
66. Tefft M, Vawter GF, Mitus A. Paravertebral "round cell" tumors in children. Radiology 1969;92(7): 1501–1509.
67. Soule EH, Newton W Jr, Moon TE, Tefft M. Extraskeletal Ewing's sarcoma: a preliminary review of 26 cases encountered in the Intergroup Rhabdomyosarcoma Study. Cancer 1978;42(1): 259–264.
68. Fink IJ, Kurtz DW, Cazenave L, et al. Malignant thoracopulmonary small-cell ("Askin") tumor. AJR Am J Roentgenol 1985;145(3):517–520.
69. Hoffer FA. Primary skeletal neoplasms: osteosarcoma and Ewing sarcoma. Top Magn Reson Imaging 2002;13(4):231–239.
70. Javery O, Krajewski K, O'Regan K, et al. A to Z of extraskeletal Ewing sarcoma family of tumors in adults: imaging features of primary disease, metastatic patterns, and treatment responses. AJR Am J Roentgenol 2011;197(6):W1015–W1022.
71. Venkitaraman R, George MK, Ramanan SG, Sagar TG. A single institution experience of combined modality management of extra skeletal Ewings sarcoma. World J Surg Oncol 2007;5:3.
72. Kushner BH, Hajdu SI, Gulati SC, Erlandson RA, Exelby PR, Lieberman PH. Extracranial primitive neuroectodermal tumors: the Memorial Sloan-Kettering Cancer Center experience. Cancer 1991;67(7):1825–1829.
73. Kennedy JG, Eustace S, Caulfield R, Fennelly DJ, Hurson B, O'Rourke KS. Extraskeletal Ewing's sarcoma: a case report and review of the literature. Spine 2000;25(15):1996–1999.
74. Rose JS, Hermann G, Mendelson DS, Ambinder EP. Extraskeletal Ewing sarcoma with computed tomography correlation. Skeletal Radiol 1983;9(4): 234–237.
75. Harimaya K, Oda Y, Matsuda S, Tanaka K, Chuman H, Iwamoto Y. Primitive neuroectodermal tumor and extraskeletal Ewing sarcoma arising primarily around the spinal column: report of four cases and a review of the literature. Spine 2003;28 (19):E408–E412.
76. Meister P, Gokel JM. Extraskeletal Ewing's sarcoma. Virchows Arch A Pathol Anat Histol 1978;378 (2):173–179.
77. Robbin MR, Murphey MD, Jelinek JS, Temple HT. Imaging of soft tissue Ewing sarcoma and primitive neuroectodermal tumor [abstr]. Radiology 1998;209(P):311.
78. Watanabe N, Kawano M, Takada M, et al. F-18 FDG PET imaging in a primitive neuroectodermal tumor. Clin Nucl Med 2006;31(8):484–485.
79. Demir MK, Koşar F, Sanli Y, Esmaeilzadeh S, Urer HN. 18F-FDG PET-CT features of primary primitive neuroectodermal tumor of the chest wall. Diagn Interv Radiol 2009;15(3):172–175.
80. Musana KA, Raja S, Cangelosi CJ, Lin YG. FDG PET scan in a primitive neuroectodermal tumor. Ann Nucl Med 2006;20(3):221–225.
81. Winer-Muram HT, Kauffman WM, Gronemeyer SA, Jennings SG. Primitive neuroectodermal tumors of the chest wall (Askin tumors): CT and MR findings. AJR Am J Roentgenol 1993;161(2): 265–268.
82. Burge HJ, Novotny DB, Schiebler ML, Delany DJ, McCartney WH. MRI of Askin's tumor: case report at 1.5 T. Chest 1990;97(5):1252–1254.
83. Chen J, Chang J, Lew P, Vasinrapee P, Shim JJ. Nuclear scintigraphy findings for Askin tumor with In111-pentetreotide, Tc99m-MIBI and F18-FDG. J Radiol Case Rep 2012;6(10):32–39.
84. Barrett D, Fish JD, Grupp SA. Autologous and allogeneic cellular therapies for high-risk pediatric solid tumors. Pediatr Clin North Am 2010;57(1): 47–66.
85. Ludwig JA. Ewing sarcoma: historical perspectives, current state-of-the-art, and opportunities for targeted therapy in the future. Curr Opin Oncol 2008;20(4):412–418.
86. Jain S, Kapoor G. Chemotherapy in Ewing's sarcoma. Indian J Orthop 2010;44(4):369–377.
87. Balamuth NJ, Womer RB. Ewing's sarcoma. Lancet Oncol 2010;11(2):184–192.
88. Schwab JH, Springfield DS, Raskin KA, Mankin HJ, Hornicek FJ. What's new in primary bone tumors. J Bone Joint Surg Am 2012;94(20): 1913–1919.
89. Gibbs CP Jr, Weber K, Scarborough MT. Malignant bone tumors. Instr Course Lect 2002;51: 413–428.
90. Mankin HJ. Ewing sarcoma. Curr Opin Orthop 2000;11(6):479–485.
91. Parida L, Fernandez-Pineda I, Uffman J, et al. Clinical management of Ewing sarcoma of the bones of the hands and feet: a retrospective single-institution review. J Pediatr Surg 2012;47(10): 1806–1810.
92. Sluga M, Windhager R, Lang S, et al. The role of surgery and resection margins in the treatment of Ewing's sarcoma. Clin Orthop Relat Res 2001; (392):394–399.
93. Krasin MJ, Davidoff AM, Rodriguez-Galindo C, et al. Definitive surgery and multiagent systemic therapy for patients with localized Ewing sarcoma family of tumors: local outcome and prognostic factors. Cancer 2005;104(2):367–373.
94. Bacci G, Balladelli A, Forni C, et al. Adjuvant and neoadjuvant chemotherapy for Ewing sarcoma family tumors in patients aged between 40 and 60: report of 35 cases and comparison of results with 586 younger patients treated with the same protocols in the same years. Cancer 2007;109(4): 780–786.

95. Bacci G, Longhi A, Barbieri E, et al. Second malignancy in 597 patients with Ewing sarcoma of bone treated at a single institution with adjuvant and neoadjuvant chemotherapy between 1972 and 1999. J Pediatr Hematol Oncol 2005;27(10):517–520.
96. Lee JA, Kim DH, Cho J, et al. Treatment outcome of Korean patients with localized Ewing sarcoma family of tumors: a single institution experience. Jpn J Clin Oncol 2011;41(6):776–782.
97. Bacci G, Longhi A, Briccoli A, Bertoni F, Versari M, Picci P. The role of surgical margins in treatment of Ewing's sarcoma family tumors: experience of a single institution with 512 patients treated with adjuvant and neoadjuvant chemotherapy. Int J Radiat Oncol Biol Phys 2006;65(3):766–772.
98. Pradhan A, Grimer RJ, Spooner D, et al. Oncological outcomes of patients with Ewing's sarcoma: is there a difference between skeletal and extraskeletal Ewing's sarcoma? J Bone Joint Surg Br 2011;93(4):531–536.
99. Burnet NG, Bliss JM, Harmer CL. The impact of radiotherapy dose on local control of Ewing's sarcoma of bone. Sarcoma 1997;1(1):31–38.
100. Rodriguez-Galindo C, Spunt SL, Pappo AS. Treatment of Ewing sarcoma family of tumors: current status and outlook for the future. Med Pediatr Oncol 2003;40(5):276–287.
101. Koontz BF, Clough RW, Halperin EC. Palliative radiation therapy for metastatic Ewing sarcoma. Cancer 2006;106(8):1790–1793.
102. Subbiah V, Ludwig JA. Review: Ewing sarcoma treatment—a role for bisphosphonates? Clin Adv Hematol Oncol 2010;8(7):503–504.
103. Paulino AC. Late effects of radiotherapy for pediatric extremity sarcomas. Int J Radiat Oncol Biol Phys 2004;60(1):265–274.
104. Pritchard DJ. Indications for surgical treatment of localized Ewing's sarcoma of bone. Clin Orthop Relat Res 1980;(153):39–43.
105. Rodríguez-Galindo C, Navid F, Liu T, Billups CA, Rao BN, Krasin MJ. Prognostic factors for local and distant control in Ewing sarcoma family of tumors. Ann Oncol 2008;19(4):814–820.
106. Dunst J, Jürgens H, Sauer R, et al. Radiation therapy in Ewing's sarcoma: an update of the CESS 86 trial. Int J Radiat Oncol Biol Phys 1995;32(4):919–930.
107. Ozaki T, Hillmann A, Hoffmann C, et al. Significance of surgical margin on the prognosis of patients with Ewing's sarcoma: a report from the Cooperative Ewing's Sarcoma Study. Cancer 1996;78(4):892–900.
108. Ahrens S, Hoffmann C, Jabar S, et al. Evaluation of prognostic factors in a tumor volume-adapted treatment strategy for localized Ewing sarcoma of bone: the CESS 86 experience. Cooperative Ewing Sarcoma Study. Med Pediatr Oncol 1999;32(3):186–195.
109. Grier HE, Krailo MD, Tarbell NJ, et al. Addition of ifosfamide and etoposide to standard chemotherapy for Ewing's sarcoma and primitive neuroectodermal tumor of bone. N Engl J Med 2003;348(8):694–701.
110. Bacci G, Longhi A, Ferrari S, et al. Pattern of relapse in 290 patients with nonmetastatic Ewing's sarcoma family tumors treated at a single institution with adjuvant and neoadjuvant chemotherapy between 1972 and 1999. Eur J Surg Oncol 2006;32(9):974–979.
111. Esiashvili N, Goodman M, Marcus RB Jr. Changes in incidence and survival of Ewing sarcoma patients over the past 3 decades: Surveillance Epidemiology and End Results data. J Pediatr Hematol Oncol 2008;30(6):425–430.
112. Ginsberg JP, Goodman P, Leisenring W, et al. Long-term survivors of childhood Ewing sarcoma: report from the Childhood Cancer Survivor Study. J Natl Cancer Inst 2010;102(16):1272–1283.
113. Haeusler J, Ranft A, Boelling T, et al. The value of local treatment in patients with primary, disseminated, multifocal Ewing sarcoma (PDMES). Cancer 2010;116(2):443–450.
114. Thorpe SW, Weiss KR, Goodman MA, Heyl AE, McGough RL. Should aggressive surgical local control be attempted in all patients with metastatic or pelvic Ewing's sarcoma? Sarcoma 2012;2012:953602.
115. Wilkins RM, Pritchard DJ, Burgert EO Jr, Unni KK. Ewing's sarcoma of bone: experience with 140 patients. Cancer 1986;58(11):2551–2555.
116. Davies AM, Makwana NK, Grimer RJ, Carter SR. Skip metastases in Ewing's sarcoma: a report of three cases. Skeletal Radiol 1997;26(6):379–384.
117. Potratz J, Dirksen U, Jürgens H, Craft A. Ewing sarcoma: clinical state-of-the-art. Pediatr Hematol Oncol 2012;29(1):1–11.
118. Miser JS, Krailo MD, Tarbell NJ, et al. Treatment of metastatic Ewing's sarcoma or primitive neuroectodermal tumor of bone: evaluation of combination ifosfamide and etoposide—a Children's Cancer Group and Pediatric Oncology Group study. J Clin Oncol 2004;22(14):2873–2876.
119. Huang HY, Illei PB, Zhao Z, et al. Ewing sarcomas with p53 mutation or p16/p14ARF homozygous deletion: a highly lethal subset associated with poor chemoresponse. J Clin Oncol 2005;23(3):548–558.

120. Huang SF, Chiang JH, Jan HC, Chou SJ, Chen TK, Chen TH. Intra-abdomen Ewing's sarcoma. ANZ J Surg 2011;81(5):377–378.
121. Contesso G, Llombart-Bosch A, Terrier P, et al. Does malignant small round cell tumor of the thoracopulmonary region (Askin tumor) constitute a clinicopathologic entity? An analysis of 30 cases with immunohistochemical and electron-microscopic support treated at the Institute Gustave Roussy. Cancer 1992;69(4):1012–1020.
122. Rodriguez-Galindo C, Billups CA, Kun LE, et al. Survival after recurrence of Ewing tumors: the St Jude Children's Research Hospital experience, 1979-1999. Cancer 2002;94(2):561–569.
123. Wagner LM, McAllister N, Goldsby RE, et al. Temozolomide and intravenous irinotecan for treatment of advanced Ewing sarcoma. Pediatr Blood Cancer 2007;48(2):132–139.
124. Dunst J, Ahrens S, Paulussen M, et al. Second malignancies after treatment for Ewing's sarcoma: a report of the CESS-studies. Int J Radiat Oncol Biol Phys 1998;42(2):379–384.
125. Fuchs B, Valenzuela RG, Petersen IA, Arndt CA, Sim FH. Ewing's sarcoma and the development of secondary malignancies. Clin Orthop Relat Res 2003;(415):82–89.
126. Tucker MA, D'Angio GJ, Boice JD Jr, et al. Bone sarcomas linked to radiotherapy and chemotherapy in children. N Engl J Med 1987;317(10):588–593.
127. Cotterill SJ, Ahrens S, Paulussen M, et al. Prognostic factors in Ewing's tumor of bone: analysis of 975 patients from the European Intergroup Cooperative Ewing's Sarcoma Study Group. J Clin Oncol 2000;18(17):3108–3114.
128. Schleiermacher G, Peter M, Oberlin O, et al. Increased risk of systemic relapses associated with bone marrow micrometastasis and circulating tumor cells in localized Ewing tumor. J Clin Oncol 2003;21(1):85–91.
129. Taber DS, Libshitz HI, Cohen MA. Treated Ewing sarcoma: radiographic appearance in response, recurrence, and new primaries. AJR Am J Roentgenol 1983;140(4):753–758.
130. Ehara S. Ewing sarcoma: changes after radiation and chemotherapy [in Japanese]. Nippon Igaku Hoshasen Gakkai Zasshi 1990;50(8):928–937.
131. Daldrup-Link HE, Franzius C, Link TM, et al. Whole-body MR imaging for detection of bone metastases in children and young adults: comparison with skeletal scintigraphy and FDG PET. AJR Am J Roentgenol 2001;177(1):229–236.
132. Hawkins DS, Schuetze SM, Butrynski JE, et al. [18F]Fluorodeoxyglucose positron emission tomography predicts outcome for Ewing sarcoma family of tumors. J Clin Oncol 2005;23(34):8828–8834.
133. Gerth HU, Juergens KU, Dirksen U, Gerss J, Schober O, Franzius C. Significant benefit of multimodal imaging: PET/CT compared with PET alone in staging and follow-up of patients with Ewing tumors. J Nucl Med 2007;48(12):1932–1939.
134. Arush MW, Israel O, Postovsky S, et al. Positron emission tomography/computed tomography with 18fluoro-deoxyglucose in the detection of local recurrence and distant metastases of pediatric sarcoma. Pediatr Blood Cancer 2007;49(7):901–905.
135. Abudu A, Davies AM, Pynsent PB, et al. Tumour volume as a predictor of necrosis after chemotherapy in Ewing's sarcoma. J Bone Joint Surg Br 1999;81(2):317–322.
136. Meyer JS, Nadel HR, Marina N, et al. Imaging guidelines for children with Ewing sarcoma and osteosarcoma: a report from the Children's Oncology Group Bone Tumor Committee. Pediatr Blood Cancer 2008;51(2):163–170.
137. MacVicar AD, Olliff JF, Pringle J, Pinkerton CR, Husband JE. Ewing sarcoma: MR imaging of chemotherapy-induced changes with histologic correlation. Radiology 1992;184(3):859–864.
138. van der Woude HJ, Bloem JL, Verstraete KL, Taminiau AH, Nooy MA, Hogendoorn PC. Osteosarcoma and Ewing's sarcoma after neoadjuvant chemotherapy: value of dynamic MR imaging in detecting viable tumor before surgery. AJR Am J Roentgenol 1995;165(3):593–598.
139. Shapeero LG, Vanel D. Imaging evaluation of the response of high-grade osteosarcoma and Ewing sarcoma to chemotherapy with emphasis on dynamic contrast-enhanced magnetic resonance imaging. Semin Musculoskelet Radiol 2000;4(1):137–146.
140. Shapeero LG, Henry-Amar M, Vanel D. Response of osteosarcoma and Ewing sarcoma to preoperative chemotherapy: assessment with dynamic and static MR imaging and skeletal scintigraphy. Invest Radiol 1992;27(11):989–991.
141. Reichardt W, Juettner E, Uhl M, Elverfeldt DV, Kontny U. Diffusion-weighted imaging as predictor of therapy response in an animal model of Ewing sarcoma. Invest Radiol 2009;44(5):298–303.

RadioGraphics

From the Radiologic Pathology Archives
Ewing Sarcoma Family of Tumors: Radiologic-Pathologic Correlation

Mark D. Murphey, MD • Lien T. Senchak, MD • Pramod K. Mambalam, MD • Chika I. Logie, MD • Mary K. Klassen-Fischer, MD • Mark J. Kransdorf, MD

RadioGraphics 2013; 33:803–831 • **Published online** 10.1148/rg.333135005 • **Content Codes:** MK MR OI PD

Page 804
Thus, it is now nearly universally agreed that Ewing sarcoma, PNET, and Askin tumor are cytogenetically closely related if not identical lesions on a morphologic continuum, which is referred to as the Ewing sarcoma family of tumors.

Page 806
The typical cytogenetic aberration, identified in 85%–95% of lesions, is the nonrandom reciprocal translocation between chromosomes 11 and 22 (t[11;22][q24;q12]).

Pages 806
Bone destruction with a moth-eaten to permeative pattern is seen in 76%–82% of lesions, and a wide zone of transition (poor margination) is seen in 96% of lesions.

Page 813
MR imaging of Ewing sarcoma of bone reveals marrow replacement (100%) and cortical destruction (92%), with an associated soft-tissue mass in 96% of cases.

Page 820
After biopsy to confirm the diagnosis, therapy primarily involves initial use of neoadjuvant chemotherapy for the purpose of eliminating micrometastases and reducing the size of the primary tumor.